UiT The Arctic University of Norway

Faculty of Science and Technology

Modeling and Analyzing of Inverters for Controlling Voltage and Frequency in an Islanded Microgrid

Mazhar Ali Khan

Master's thesis in Electrical Engineering…ELE-3900…May 2021

ABSTRACT

Recently, the growth of inverter-based generations (IBGs) like solar photovoltaic (PV) and wind turbine generators in the form of microgrids (MGs) has been increasing. However, control of voltage and frequency becomes a challenging task for MGs especially when they operate in an islanded mode, due to the inherent low-inertia feature of IBGs compared to a grid-tied mode where there is a grid support. This thesis deals with modeling and analyzing of inverters capable of controlling voltage and frequency through external conventional droop control for the islanded operation of MG. In this thesis, a state space model is developed for a voltage source inverter with droop control. Moreover, non-linear models for the inverters in single and parallel cases with droop control are developed and the results are verified in different load scenarios. The results show a good performance of the projected control, both in the isolated operation of an inverter supplying a load, and in the parallel operation of isolated inverters, where there is power sharing to properly feed the load. MATLAB/Simulink environment is used for the work.

ACKNOWLEDGEMENT

My profound gratitude goes out to my family for their support throughout the course of my study. I will also say a big thank you to my family for their encouragement at every stage of my life.

I would also like to show my sincere gratitude to my supervisor, Associate Professor Pawan Sharma for his guidance, support, patience, motivation, assistance, and technical guidance throughout the course of this work.

My sincere gratitude goes out to Doctoral Student Shwetank Agrawal of Indian Institute of Technology, Roorkee, India.

I would also like to express my appreciation for the invaluable guidance provided to me by Associate Professor Bjarte Hoff and Post-Doctoral Fellow Chittaranjan Pradhan.

In the end, I would like to express my gratitude to Doctoral Student Hussein Mahdi for always making himself available when I needed help.

Table of Contents

List of Tables

List of Figures

LIST OF ABBREVIATIONS

MGs	Microgrids
MMGs	Multi-microgrids
DG	Distributed generation
RESs	Renewable energy sources
3S	Small signal stability
CHP	Combines heat and power
PV	Photo-voltaic
DC-MG	DC microgrid
AC-MG	AC microgrid
EVs	Electric vehicles
PCC	Point of common coupling
MMPT	Maximum power point tracking
MP	Market price
UPS	Uninterruptible power supply
P-V	Active Power-voltage curve
Q-V	Reactive power-voltage curve
DSTATCOM	Distribution static compensator
VSC	Voltage source control
VCVSI	Voltage control voltage source inverter
CCVSI	Current controlled voltage source inverter
MGCC	Microgrid control center
PLL	Phase-locked loop

VSI	Voltage source inverter
THD	Total hormonic distortion
LC	Local control
CPLs	Constant power loads
ESS	Energy storage system
LCL	Inductive-capacitive-inductive
URDC	Universal robust droop controller
QPR	Quasi-proportional resonant
CCM	Current control method
BPCs	Bidirectional power converters
GDC	Generalized droop control
PSO	Particle swarm optimization
GA	Genetic algorithm
EMS	Energy management system
CLC	Central limit control
3C	Circular chain control
CPPs	Central power plants
PQ	Power quality

LIST OF SYMBOLS

V_{cc}	DC bus Voltage
d_a	Phase a modulation index
d_b	Phase b modulation index
d_c	Phase c modulation index
$\vec{\imath}_{c,abc}$	Output inverter phase currents
$\vec{\imath}_{g,abc}$	Output load phase currents
$\vec{v}_{cf,abc}$	LCL capacitors voltage vector connected in the abc phases
$\vec{v}_{cd,abc}$	damping branch capacitors voltages vector connected in the abc phases

$v_{n,c}$	Coupling DC side voltage
$v_{n,g}$	Coupling grid voltage
v_{gc}	Voltage between $v_{n,g}$ and $v_{n,c}$
v_{fc}	Voltage between $v_{n,g}$ and $v_{n,f}$
$\vec{u}$	Vector with unitary components
$[\mathbf{L_c}]$, $[\mathbf{L_g}]$	Inductances matrix connected to the inverter and the inductances connected to the power grid
$[\mathbf{C_d}]$	Damping capacitances matrix
$\theta_{e,g}$	Angle between phases
L_c	Filter inductor on the inverter side
L_g	Filter inductor on the grid side
C_f	Filter capacitor
C_d	Filter damping capacitor
ω_g	Grid angular frequency
f_{load}	Load frequency
f_{si}	Inverter Switching Frequency
$\Delta i_{c,max}$	Current ripple
α_C	Ratio factor of Capacitors C_f and C_d
α_L	Relation Factor of Inductances $L_c$and L_g
f_{res}	Filter Resonance Frequency
K_{ci}	Current Controller Gain
ω_{zi}	Current controller zero angular frequency
PM	Phase Margin
ω_{ci}	Current control cut-off angular frequency
f_{ci}	Current control cut-off frequency

p	Instantaneous output active power
q	Instantaneous output reactive power
v_{cd}, v_{cq}	Inverter output voltages
$i_{od},\ i_{oq}$	Inverter output currents
m_d, m_q	Droop coefficients
$\Delta\omega, \Delta E$	Maximum desired variatons of angular frequency and voltage
$P_{max,}\ Q_{max}$	Inverter maximum active and reactive power
$K_i, K_{pi}\ T_{ii}$	PI current controller: gains (proportional and integral) and constant integration
T_s	Sampling time
$K_v\ K_{pv}\ \ T_{iv}$	PI voltage controller: gains (proportional and integral) and constant integration

1 INTRODUCTION

1.1 Background and Motivation

In both developed and developing countries, use of distributed energy resources (DERs) at the utility grid is growing day by day. Microgrids are one of the promising solutions to integrate the various types of DERs with the utility grid. MG concept undertakes a group of loads and small scale conventional and non-conventional sources such as diesel generators, PV and wind, operate as a single, controllable device that provides both power and heat to its immediate surroundings. MG's structure coordinate DERs in a continuously more decentralized manner, reducing the grid's control load and allowing them to have their maximum benefits [1]. Microgrid implementations are projected to enhance PQ, lower radiations, reduce network bottleneck and power losses, boost energy efficiency, and probably enhance economics of the system. However, this MG has its own challenges in the implementation [1]. Control of voltage and frequency becomes a challenge task for MGs especially when they operate in an islanded mode due to the inherent low-inertia feature of inverter-based generations compared to a grid-connected mode. This thesis deals with modeling and analyzing of inverters capable of controlling voltage and frequency through external conventional droop control for the islanded operation of MG. In addition, the purpose of the work is to develop a general state space model for the entire system, as a single closed-loop system, which allows for a unique analysis of the system as well as the stability analysis of closed-loop operation.

This thesis is a small task of a work package for an ongoing research project funded by Department of Science and Technology (DST), India and Mission Innovation (MI), titled as" Design and Development of Hybrid Renewable Energy Micro-grid with Value Chain Applications for Agricultural and Dairy Farm" duration, 2018-2021, partners UiT, Norway and IIT Roorkee, India. This project deals with the design and development of an ac-dc MG and integration with main grid.

1.2 Problem Statement

MGs can function in two modes: connected to a grid or in islanding mode. MG will be said to be in islanding condition, when a microgrid or a part of the power grid, comprising of DG

sources, converters, and loads, is cut off from the main utility grid. Grid-connected mode is the situation in which MG can couple itself with main utility grid through point of common coupling (PCC) to purchase electricity in case of electricity shortage at their own end and sell electricity during surplus situation. Figure 1 shows the basic sketch of a microgrid.

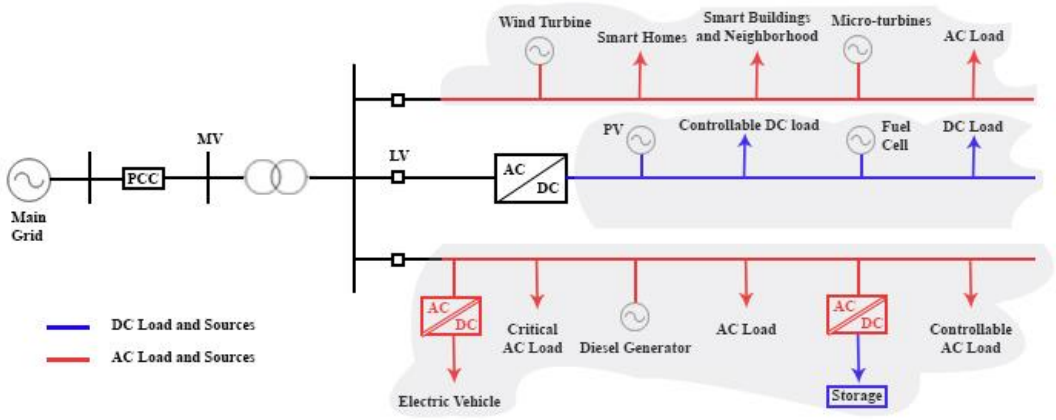

Figure 1 Basic sketch of a microgrid

These modern power systems present several factors that vary from those previously considered in the design and operation of traditional power systems controlled by massive synchronous generators powered by hydro or thermal turbines. Implementing intermittent energy sources, for example, necessitates the creation of new power dispatch and control strategies capable of compensating for such intermittency by controlling and organizing the integration of ESS throughout the MG. The difficulty rises as the penetration of non-dispatchable sources deepens. Stability problems in MGs can be attributed to a variety of factors, including grid characteristics and topologies, electric element values, and the direction and magnitude of power flows, among others. The reasons behind the microgrid stability issues could be the technology of power reaching, harmonic-suppression, and the stability of electronic cascaded systems are among the factors. The effects of droop control gains, line impedance, and load variations on MG voltage and frequency characteristics also need to be addressed.

The aim of this thesis is the modeling of inverters capable of controlling voltage and frequency through external conventional droop control for the islanded/isolated operation of a microgrid. In addition, the purpose of the work is to develop a general state space model for the entire

system, as a single closed-loop system, which allows for a unique analysis of the system as well as the stability analysis of closed-loop operation.

1.2.1 Thesis Contributions

These contributions of the thesis are presented here verbatim. They were divided into two main parts

Part 1.

(a) Simulating a three-phase inverter having a 120 DC Bus and output of 400v, 50Hz under different loading conditions.

(b) Adding Droop Characteristics in the three-phase inverter and see the effect under different loading conditions.

(c) State Space modeling of the three-phase inverter having droop characteristics.

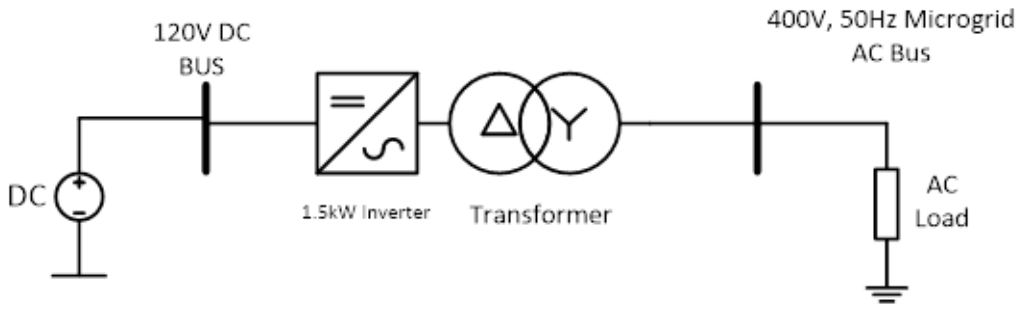

Figure 2 Single three-phase inverter

Part 2.

(a) Simulating the three phase parallel inverters having droop characteristics.

(b) Ensuring power sharing between the two inverters with changes in load.

(c) State Space modeling of the parallel model with droop characteristics

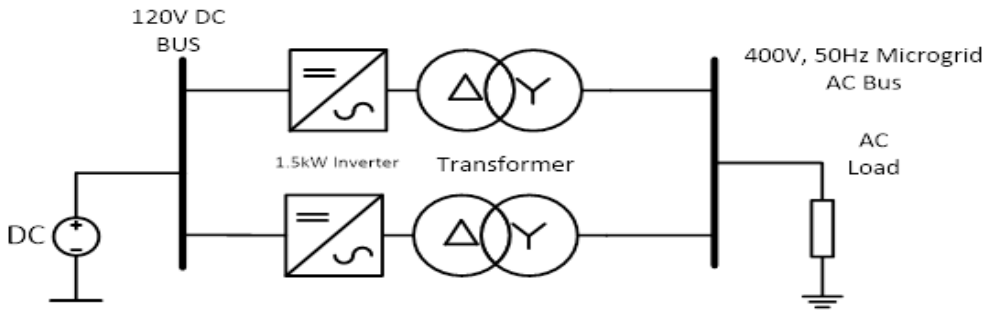

Figure 3 Two parallel three-phase inverters

1.2.2 Thesis Limitations

Due to time limitation, some definitions were adopted.

- One of the assumptions used was for isolated load to be treated as resistive in the tests and results extraction (although the generic model presents it as a Z impedance).
- Another point was the definition of the LCL filter, since it is most used for this type of application, but it could still be compared with other topologies.
- Similarly, the topology of the 2L inverter (two levels) was used due to the low power applications of the inverters.
- Moreover, the microgrid was assumed to be isolated and the inverter operation is considered only for isolated/standalone mode.
- The COVID-19 pandemic adversely affected the work during the thesis.

1.3 Thesis Structure and Layout

This project is structured as follows:

- **Chapter 1**- An introduction is made to the research topic and the objectives.
- **Chapter 2**- Introduction to three phase inverters in microgrids from operation and control perspectives and concepts regarding parallel operation and control of three phase inverters. Additionally, power sharing strategies and droop control are introduced.

- **Chapter 3**- Necessary definitions are presented and mathematical models are developed.
- **Chapter 4**- Non-linear simulations are presented for single inverter and parallel inverters. State space models with convetional droop control are developed for both cases.
- **Chapter 5**- Conclusions are made. A reflection is given on the work done and possibilities for future work are proposed.

2 LITERATURE REVIEW

This chapter is systematized as: Section 2.1 discusses the literature on three phase inverters in microgrid from operation and control perspectives and parallel operation and control of three phase inverters. Section 2.2 discusses the power sharing control strategies in microgrid paradigm. Section 2.3 discusses the droop control and its different strategies from operation and control perspectives of microgrids. Finally, section 2.5 discusses the background of small signal stability and literature of droop control strategies for handling the small signal stabilities in microgrids.

2.1 Three Phase Inverters in Microgrid: From Operation and Control Perspectives

In comparison to large, CPPs, the DG system (Microgrid system) provides better power quality and reliability for industries that need constant power. Power converter advancements, combined with classy high-performance controllers, have made it possible to integrate various types of renewable energy sources into the grid. PWM inverters have traditionally been used to link green energy sources to the power grid. It should be able to run in both grid-connected and islanding modes. The grid-connected inverter in the DG system is usually worked to inject preset true- and reactive-powers to the main grid during grid-connected operation, which is the current control mode in synchronization with the grid voltage. Authors in [2] suggested a predictive current controller strategy in a grid-connected single-phase inverter with LCL filter that is resilient to part parameter variations and introduces computation delay time. The authors of [3] proposed a new robust predictive current controller for three-phase inverters that provides robustness against these two factors while retaining the quick response typical of a deadbeat

controller. The authors of [4] used a discrete domain pole location method to create a PI state space current control system that can be tuned simply by providing the most appropriate system parameters, namely LCL filter elements and control frequency. Researchers in [5] proposed a grid current control method for grid-connected operation and an inverter voltage control method based on the PLL for deliberate islanding operation at three-phase grid-connected inverters. To synchronize the step of inverter output voltage with a grid voltage at the grid-connected operation or produce a desired inverter output voltage at the islanding operation, the authors used a PLL controller based on the pq principle with a simple P-controller. A new unified control strategy based on URDC and QPR regulator for MG parallel operation using a CCM was proposed to ensure equal power sharing among parallel controlled inverters during all MG operating modes.

2.1.1 Parallel Operation and Control of Three Phase Inverters

RE power generation is progressively being incorporated into the grid in AC-MG through power electronic converters like DC-AC inverters, which are often run in parallel. These inverters are often used by droop control while an MG is running in islanded mode to achieve adequate load-sharing efficiency and match the demand of local loads to ensure system reliability. Using network-based control, system output for three-phase inverter parallel operation in a droop-controlled AC-MG will theoretically be improved, with additional advantages for the expansion of other control strategies in microgrids. Authors in [6] examined in islanded mode of an AC-MG with paralleled inverters a thorough study of network-based control strategy with high robustness and broad time-scale compatibility. It is tested that good power-sharing can be achieved under unsatisfactory connectivity conditions based on a theoretical assessment of time-delay and data dropouts. The MG's function is primarily determined by the organizational (control) scheme that is used to run it. The MG's control scheme is primarily classified into two groups. Droop control schemes are the first type, whereas distributed control schemes are the second. The authors of [7] proposed a novel method for interfacing parallel inverters based on P-F/Q-V droop function. Researchers in [8] proposed a revolutionary operational system to steady the V&f in the MG under a variety of loading conditions, including variable balanced loads, variable unbalanced loads, and nonlinear loads, based on the self-adaptive PI controller. A 3C technique for inverters in parallel operation was

analyzed to obtain an equivalent current distribution. It has been shown that a system using the suggested technique can handle a wide range of loads. The suggested plan has a high degree of current monitoring. One of the parallel BPCs controls the DC bus voltage, while the other BPCs transfer power between the AC and DC grid. A string converter formed by a few series-connected micro-converters in proposed method, and power sharing between parallel string converters is achieved using droop control. A utility linked multiple microgrids method was proposed, and a solution was proposed to manage the back-to-back connections without sacrificing the microgrids' autonomy. Theoretical evaluations of time-delay and data dropouts have been conducted, and it has been shown that effective power-sharing can be achieved even under poor connectivity conditions. In islanded ac microgrids, parallel droop-controlled inverters with renewable energy sources are commonly used, but complex interactions among them can cause 3S issues. A new small signal fatal distinguishing model for droop-controlled inverters is introduced by researchers. A new set of terminal properties has been introduced to describe the dynamics of fundamental frequency in addition to traditional impedance and admittance. Furthermore, the parallel inverter's small-signal model is built using the terminal characteristics of individual inverters. The traditional droop characteristics has some limitations to satisfy all the characteristics of microgrid operation and control, so researchers modified the traditional droop control characteristics to satisfy the necessity of inverters operating in parallel in all voltage sources-based inverters microgrids. A double closed loop control system based on measured voltage feedback was used for inverter control in the microgrid to address the issue of voltage sags induced by the implementation of virtual impedance. When the microgrid has operating in islanded mode, authors examined the interfaced parallel inverter control using a P-F/Q-V droop control. The authors of [9] proposed a new centralized control system based on the Model Predictive Control algorithm that coordinates parallel operations of various distributed generation inverters inside a microgrid and allows for quicker calculation time for big power systems by enhancing the stable-state and transient control hitches distinctly. Finally, in [10] authors presented a recent state-of-the-art analysis of parallel power electronic inverter control methods. The advantages and disadvantages of various system architectures, their operation modes, management & control methods, and tactics have been studied and debated.

2.2 Power Sharing Control Strategies in Microgrid

The electronic converter crossing point between the loads and the micro-source serve as voltage sources in islanding mode, and they are accountable for power sharing based on their ratings and the availability of power from their respective energy sources or prime movers. The authors in [11] suggested a multi-master-slave community-based management system that combines a droop power sharing structure to take advantage of the benefits of both droop and master-slave control strategies.

Table 1 Features of conventional and improved control methods in different aspects [11].

FEATURES	DROOP	MASTER SLAVE	HYBRID
RESITIVE LINE IMPEDANCE	Large reactance circulation	No harm	No harm
POWER SHARING	Present	Not present	Present
RELIABILITY	Present	Not present	Present

The traditional droop regulation has certain drawbacks, such as a significant decrease in load voltage. The parallelly driven inverters in a traditional droop control scheme must have the same per unit production impedance. Furthermore, the relation voltage must be the same such that the load can be distributed proportionally to their respective ratings. Since the above requirements are very difficult to follow in practice, there will still be some relative load sharing failures. As a result, an improved droop control has been proposed in [12] in order to achieve error-free load sharing based on their droop ratio while avoiding the conditions mentioned above. The production active power of renewable sources is controlled by a droop control strategy to achieve truly decentralized power sharing. The adaptive droop parameters were calculated using the microgrid impedance. This method ensures efficient power sharing while also lowering line losses. While this approach enhances the active power sharing, but it ignores the reactive power sharing. Authors in [13] proposed an optimization-based strategy for adjusting control parameters by striking a balance between reactive power sharing and voltage management. A brief analysis of power sharing control approaches for islanding operation of

AC microgrid has been presented. To achieve equal current distribution in CLC mode, all modules should have the same configuration and each module should log the average current. Droop coefficients and reference frequencies were used to illustrate successful power management. A novel absolute damping factor has also been introduced to increase transient reaction and minimize reactive power flow. Researchers in [14] presents a new control scheme for islanded AC microgrids based on the Finite Control Set-Model Predictive Control strategy. To produce reference voltage for the inner loop and achieve load power sharing, droop control with simulated impedance was used. To watch the

Table 2 Different droop control strategies and the pro and cons [15].

CONTROL STRATEGY	ADVANTAGES	DISADVANTAGES
CONVENTIONAL DROOP	• Avoiding a vital communication channel. • High level of versatility and reliability.	• Slow dynamic response • Poor hormonic load sharing • Weak voltage management • Poor performance with RESs
ADAPTIVE DROOP	• Good transient response • Excellent power sharing • Good voltage and frequency regulation	• Virtual reactance needed is used to minimize the circulating power • The magnitude and phasor angle of output impedance is difficult to control • Improvement is not significant • Complicated

voltage reference and choose the best control action for the next move, an improved Finite Control Set-Model Predictive Control technique was used. The effects of communication delays are considered to ensure correct active and reactive power sharing, and multiple control

protocols are provided to restore the frequency and terminal voltage of the system to nominal range. The authors of [16] suggested a decentralized Lyapunov-based control strategy to address voltage modulation and power sharing output limitations in the islanding single-phase MG in the presence of impedance variations. The traditional droop regulation has certain drawbacks, such as a significant decrease in load voltage. This is mostly due to higher load currents and droop coefficients. Another disadvantage to the traditional droop is that a large droop coefficient improves reaction time. The researchers of [17] looked at both the traditional and enhanced droop control strategies for two parallel coupled high voltage and high-power inverters for resistive and inductive loads. A new droop strategy has been suggested in [18] to improve the accuracy of power sharing in a standard low voltage microgrid with unbalanced loads and mismatched phase impedance of feeders, based on the triple-droop-control strategy and virtual impedance concept. DC voltage harmonic frequencies have been used to construct a global vector in the DC side of hybrid microgrids and to implement an optimal droop control technique for the DC MG while maintaining power efficiency. Two important tasks for the islanding operation of AC-MGs are to proportionally share load demand among multiple parallel connected inverters and to maintain voltage and frequency stability. As a result, researchers in [19] provided a brief overview and classification of different power sharing management rules in MGs. To enhance the precision of power sharing output between parallel inverters, droop control with a secondary control loop was presented for an AC-MG in [20]. At last, Authors of [21] suggested a harmonic droop to compensate for voltage distortion induced by non-linear loads in an islanded microgrid by collaborating between separate voltage controlled DGs. P-F/Q-V droop control is the procedure employed.

2.3 Droop Control in Microgrid Operation & Control

Droop control is the key to exchanging demand power between generators in autonomous microgrids where the energy delivery grid is unavailable. In conventional synchronous generators and uninterruptible power supplies, droop control is widely used. It has the advantage of allowing each DG to run independently without the need for crucial contact. When the equivalent impedance connecting DGs to the grid in a microgrid is inductive, P-f and Q-V droop control are usually used. Many researchers have worked on different aspects of microgrids using droop controller techniques. Authors in [22] proposed a new automated droop

control approach based on a thorough examination of DC microgrid characteristics such as current sharing accuracy, voltage management, destabilizing effects of CPLs, and device reliability. The authors suggested a bidirectional droop control method for the converter in [23], which calculated the path and magnitude of the converter transmission power by measuring the power demand degree of the AC and DC sub-grid according to AC bus frequency and DC bus voltage, respectively. Researchers in [24] proposed a new adaptive droop control system based on a detailed review of the key indices used in the DC MG output and adjusted the droop slope automatically according to the load condition without using any contact relation. In [24], the authors suggested a new adaptive droop management technique for balancing the state of charge of energy storages in an islanded AC microgrid. In [25], the authors suggested a distributed coordination control system for multiple bidirectional power converters in a hybrid AC/DC microgrid that can realize the necessary power relationship between the two sub-grids and have the two sub-grids support each other, allowing the hybrid microgrid to work well in both grid-connected and islanded modes. Authors in [26] proposed an improved control system for various two-directional power converters in a hybrid microgrid operating in island mode that includes rotating current reduction and power sharing. The production active power of micro-turbines is controlled by droop control strategy to achieve completely decentralized power sharing. Authors in [27] proposed an autonomous MG comprising three DG units. PV System, which is operated in PQ control mode, and MTs, which are operated in VF control mode, were two of the DGs. In [28], the authors proposed a decentralized secondary control scheme for an MG with both VF and PQ controlled inverters. To produce the required compensation signals for frequency deviation, the proposed secondary controllers were based on identical PI controllers. The authors of [29] suggested a GDC scheme that can provide adequate control efficiency in both grid-connected and islanding modes of MG service. At last, the droop-based decoupling power of a neutral point clamped 3-level inverter in MG's islanded mode of operation is investigated in [30].

2.4 Small Signal Stability and Droop Control

In multimachine networks, small signal model research has a long tradition. Laughton and Uudrill made notable contributions in 1966 and 1968, respectively, which were mostly used for device stability research. It was recently expanded to include microgrid applications. Droop

control and 3S analysis were first demonstrated in uninterruptible power supply systems. Microgrid was also used to test the procedure. A linearized network, DGs, DG control units, and a load model are used to investigate microgrid 3S. The eigenvalue can be measured using the linearized mode while the Microgrid operates at different operating points. Renewable energy-based energy conversion systems, despite their erratic existence, have become more relevant due to environmental concerns. As a result, the microgrid principle and microgrid control methods have emerged as significant research fields in power systems. Because of its simplicity and lack of reliance on costly communication networks, the droop-based control method is more common in microgrid systems than other inverter control methods. Droop control is a form of peer control that aims to render the performance characteristic of an inverter-interfaced DG close to that of a synchronous generator with P/f droop and Q/V droop, allowing for a fair load sharing among all DG units without contact. A lot of research has been conducted in the literature on conventional and improved variant of droop control for analysis of 3S. In a microgrid, virtual impedance, angle droop, and frequency droop control are critical for device stability and load sharing among DGs. Based on traditional droop control, [31] proposed an improved droop control with voltage amplitude feedback PI control as a voltage amplitude feedback technique to improve the Q/V droop module for better DG unit output voltage amplitude control accuracy. The above-mentioned MG' 3S small signal state space model was then developed. A comparison of two commonly used grid-forming droop controls, single-loop and multi-loop droop controls is presented in presented literature. The stability of small signals on microgrids has been discussed. The transient response has been enhanced by adding simulated impedance and dynamic droop gains. Particle swarm optimization has been used to optimize the various controller parameters, maintaining stability. A sub-model of power controller, a sub-model of constant power loads, and a sub-model of network and loads have been created for a narrow signal state-space model of microgrid. The authors of [32] developed a detailed small signal state-space model of the entire microgrid, including the droop controller, network, and loads, in order to enhance the dynamic characteristics of an inverter-based microgrid. A droop-like voltage feedback controller with quadratic local voltage magnitude has been proposed, enabling circuit theoretic research techniques to be applied to the closed-loop system. A droop-like voltage feedback controller with quadratic local voltage magnitude has been proposed, enabling circuit theoretic research techniques to be applied to the closed-loop

system. In microgrids, frequency-droop gains have an important impact on stability. Authors in [33] uses qualitative analysis and small-signal methods to find a relationship between these parameters and stability margins. The authors proposed an EMS for a stand-alone droop-controlled microgrid that changes generator output power to reduce fuel consumption while maintaining stable operation. The authors of [34] implemented a novel method of sensitivity analysis, parameter tuning, and optimization with respect to 3S of grid-forming and grid-supporting droop regulated inverters in microgrids using a GA. A multi-objective optimization segmented droop control ideal for economic dispatch for a DC microgrid has been proposed to achieve a greater controllable spectrum of output/input capacity of droop-control sources. Via the study of a generalized model of several droop-control outlets, the worst point of equilibrium in the droop-control curve has been calculated. Using dynamic phasors, a new simulation method for inverter-dominated microgrids has been proposed. Finally, to cope with the variety of renewable energy sources, the authors of [35] designed a complex droop control technique to ensure optimal power sharing and improve the 3S efficiency of MG in islanding operation.

2.5 Summary

In this chapter, the state-of-the-art literature review on different aspects of three phase inverters from operation and control perspectives, parallel operation of three phases inverters, power sharing technologies and strategies, droop control and on 3S have been presented.

3 MODELING AND IMPLEMENTATION

To present the inverter model used, some definitions are needed. There are several topologies of inverters and filters in the literature, each with its advantages and disadvantages, and also classified according to the desired operation and analysis. One of the main criteria for choosing between topologies is the rated power of the inverter. Obviously, for practical application, other criteria come up, for example: maintenance, reliability and size / weight ratio.

According to [36], when dealing with AC / AC conversion, the topologies can be divided into two: indirect and direct. In the indirect case, there is a DC link that connects two converters, performing two transformations: AC - DC - AC, while in the direct case the DC link does not exist, and the transformation is AC - AC. There are numerous advantages and disadvantages

between the two topologies, however, in this case, the indirect topology will be treated, that is, that the DC link exists, and also, assuming the constant DC link, that is, assuming that the primary machine can supply all the energy demand required by the grid-side converter. This is done to focus the modeling and results for the inverter responsible for controlling the power flow to the grid in the connected case, or to control the voltage and frequency in the load, in the isolated case. In this work, the focus is the isolated operation, to highlight the performance of the droop loops, and to develop a state-space model with the intrinsic droop control in the model.

Still on topologies, the converters can be classified in 2 major categories: as VSC (Voltage Source Converter), CSC (Current Source Converter). The most commonly used topology is VSC (or VSI - Voltage Source Inverter) converters, where there is the presence of a relatively large capacitor on the DC link, which feeds the inverter circuit through a three-phase bridge. This bridge is made up of 6 switches that allow bidirectional current flow [36]. In the case of this work, the DC link can be considered as a constant voltage source.

In this work, the inverter topology of the VSI 2L type was adopted, due to the low power of the inverter, and the greater simplicity of parallelism of inverters. As the name implies, this inverter transforms the V_{dc} voltage up to two levels (V_{dc} and $-V_{dc}$). Figure 4 shows the basic topology of the inverter adopted, equipped with 2 switches for each phase, where the DC link capacitor can be considered a constant source.

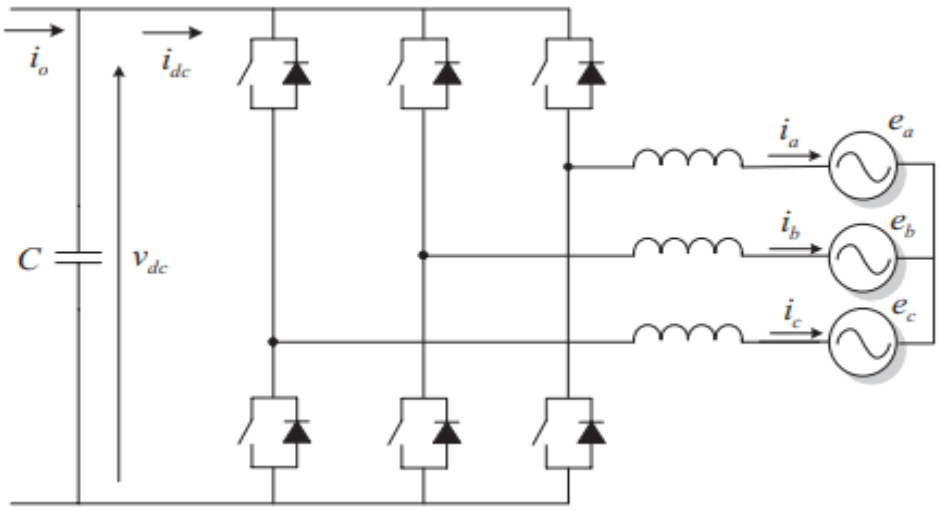

Figure 4 Grid converter topology [36]

VSC converters have unwanted harmonic injection characteristics in the grid, and to mitigate this, an output filter must be well-designed, considering factors such as: different harmonic spectrum, possible resonance conditions and variations of harmonics with the operating point. The choice of the filter must be based on its contribution to the attenuation of the harmonics. Using just a L filter (as in Figure 4), makes a large inductance needed to limit the high frequency switching ripple, which would result in a large and expensive filter. In this context, the LC and LCL type filters stand out more, as they present two and three times attenuation compared to L filter, respectively. Thus, the cost of these filters is lower, since the parameters can be lower. In this sense, the LCL filter is the most commonly used to solve this problem, and some design methods are presented in the literature. For the LCL filter design in this work, [37] and [38] are referenced. They are defined and design parameters are shown in the next sections.

3.1 Modeling of the Inverter Connected to the LCL Filter and the Load

The passive filter topology for connection to the load and the damping method were chosen due to the common use for applications focused on stability analysis. It is possible to obtain the mathematical model that represents the dynamic behavior of the inverter connected to the load through the damped LCL filter, which will be used to design the controllers voltage and current.

For this, the average model of the inverter is adopted, following [39], according to the electrical diagram illustrated in Figure 5 below.

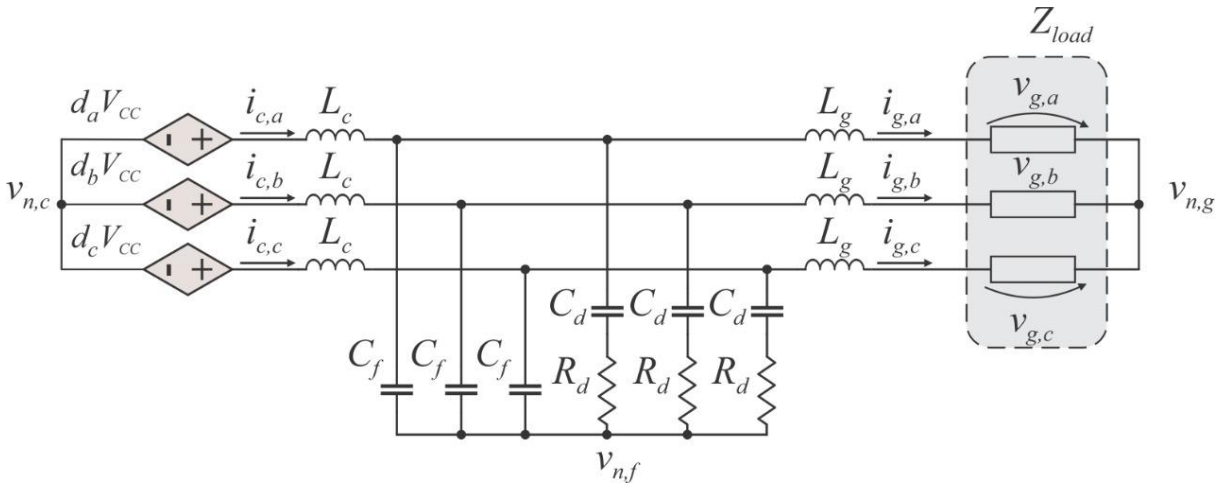

Figure 5 Electrical diagram of the equivalent circuit connected to the load [39]

From Figure 5, it is possible to obtain the voltages in abc coordinates by applying the Kirchoff's voltage law, as described by (1), (2), (3) and (4).

$$[\mathbf{L_c}]\frac{d}{dt}\vec{\imath}_{c,abc} + [\mathbf{L_g}]\frac{d}{dt}\vec{\imath}_{g,abc} = \vec{d}_{abc}V_{CC} - \vec{v}_{g,abc} - v_{gc}\vec{u} \quad (1)$$

$$[\mathbf{L_c}]\frac{d}{dt}\vec{\imath}_{c,abc} = \vec{d}_{abc}V_{CC} - \vec{v}_{cf,abc} - v_{fc}\vec{u} \quad (2)$$

$$[\mathbf{L_g}]\frac{d}{dt}\vec{\imath}_{g,abc} = \vec{v}_{cf,abc} - \vec{v}_{g,abc} - v_{gf}\vec{u} \quad (3)$$

$$[\mathbf{C_d}]\frac{d}{dt}\vec{v}_{cd,abc} = \frac{\vec{v}_{cf,abc}}{R_d} - \frac{\vec{v}_{cd,abc}}{R_d} \quad (4)$$

Where,

- $\vec{v}_{g,abc}$: is the load phase voltages vector, defined by (5);
- $\vec{\imath}_{c,abc}$: : is the output inverter phase currents, defined by (6);
- $\vec{\imath}_{g,abc}$: is the output load phase currents, defined by (7);

• $\vec{v}_{cf,abc}$: is the LCL capacitors voltage vector connected in the abc phases, defined by (8);

• $\vec{v}_{cd,abc}$: is the damping branch capacitors voltages vector connected in the abc phases, defined by (9);

• v_{gc}: is the voltage between $v_{n,g}$ and $v_{n,c}$ (see Figure 5).

• v_{fc}: is the $v_{n,f}$ and $v_{n,c}$ (see Figure 5).

• v_{gf}: is the voltage between $v_{n,g}$ and $v_{n,f}$ (see Figure 5).

• $\vec{u}$: is a vector with unitary components, defined by (10);

• R_d: the resistance of the damping branch;

• $[\mathbf{L_c}]$ and $[\mathbf{L_g}]$: are inductances matrix connected to the inverter and the inductances connected to the power grid represented in Figure 5, defined by (11) and (12);

• $[\mathbf{C_d}]$: is damping capacitances matrix represented in Figure 5, defined by (13);

$$\vec{v}_{g,abc} = [v_{g,a} \quad v_{g,b} \quad v_{g,c}]^T = Z_{load}[i_{g,a} \quad i_{g,b} \quad i_{g,c}]^T \tag{5}$$

$$\vec{i}_{c,abc} = [i_{c,a} \quad i_{c,b} \quad i_{c,c}]^T \tag{6}$$

$$\vec{i}_{g,abc} = [i_{g,a} \quad i_{g,b} \quad i_{g,c}]^T \tag{7}$$

$$\vec{v}_{cf,abc} = [v_{cf,a} \quad v_{cf,b} \quad v_{cf,c}]^T \tag{8}$$

$$\vec{v}_{cd,abc} = [v_{cd,a} \quad v_{cd,b} \quad v_{cd,c}]^T \tag{9}$$

$$\vec{u} = [1 \quad 1 \quad 1]^T \tag{10}$$

$$[\mathbf{L_c}] = \begin{bmatrix} L_c & 0 & 0 \\ 0 & L_c & 0 \\ 0 & 0 & L_c \end{bmatrix} \tag{11}$$

$$[\mathbf{L_g}] = \begin{bmatrix} L_g & 0 & 0 \\ 0 & L_g & 0 \\ 0 & 0 & L_g \end{bmatrix} \quad (12)$$

$$[\mathbf{C_d}] = \begin{bmatrix} C_d & 0 & 0 \\ 0 & C_d & 0 \\ 0 & 0 & C_d \end{bmatrix} \quad (13)$$

In the same way, applying Kirchoff's currents law in the electrical diagram illustrated in Figure 4, we obtain the expression that relates the inverter's output current and the current injected into the load. Thus,

$$[\mathbf{C_f}] \frac{d}{dt} \vec{v}_{cf,abc} = \vec{\imath}_{c,abc} - \vec{\imath}_{g,abc} - \left(\frac{\vec{v}_{cf,abc}}{R_d} - \frac{\vec{v}_{cd,abc}}{R_d} \right) \quad (14)$$

Where,

• $[\mathbf{C_f}]$: is the matrix of the LCL filter capacitances represented in Figure 5, defined by (15);

$$[\mathbf{C_f}] = \begin{bmatrix} C_f & 0 & 0 \\ 0 & C_f & 0 \\ 0 & 0 & C_f \end{bmatrix} \quad (15)$$

Thus, from the mathematical deductions made above, the abc coordinate model is obtained, which governs the dynamic behavior of the inverter connected to the load through the damped LCL filter.

$$\begin{cases} [\mathbf{L_c}]\frac{d}{dt}\vec{\imath}_{c,abc} + [\mathbf{L_g}]\frac{d}{dt}\vec{\imath}_{g,abc} = \vec{d}_{abc}V_{CC} - \vec{v}_{g,abc} - v_{gc}\vec{u} \\ [\mathbf{L_c}]\frac{d}{dt}\vec{\imath}_{c,abc} = \vec{d}_{abc}V_{CC} - \vec{v}_{cf,abc} - v_{fc}\vec{u} \\ [\mathbf{L_g}]\frac{d}{dt}\vec{\imath}_{g,abc} = \vec{v}_{cf,abc} - \vec{v}_{g,abc} - v_{gf}\vec{u} \\ [\mathbf{C_d}]\frac{d}{dt}\vec{v}_{cd,abc} = \frac{\vec{v}_{cf,abc}}{R_d} - \frac{\vec{v}_{cd,abc}}{R_d} \\ [\mathbf{C_f}]\frac{d}{dt}\vec{v}_{cf,abc} = \vec{\imath}_{c,abc} - \vec{\imath}_{g,abc} - \left(\frac{\vec{v}_{cf,abc}}{R_d} - \frac{\vec{v}_{cd,abc}}{R_d}\right) \end{cases} \tag{16}$$

3.1.1 Coordinate Modeling (dq0)

Once the inverter model connected to the load has been defined by means of the passive LCL filter damped in abc coordinates, it is convenient to apply the Park transform to obtain the model in dq0 synchronous coordinates, as performed for the entire system presented in the previous section. In addition, it is possible to maintain the simplicity of the control strategy, where PI type controllers can be used to control the current injected into the electrical grid or load. Therefore, the Park transform and the inverse used are described by (17) and (18), respectively.

$$\underbrace{\begin{bmatrix} f_d \\ f_q \\ f_0 \end{bmatrix}}_{\vec{f}_{dq0}} = \underbrace{\frac{2}{3}\begin{bmatrix} cos(\theta_{e,g}) & cos(\theta_{e,g} - \frac{2\pi}{3}) & cos(\theta_{e,g} + \frac{2\pi}{3}) \\ -sin(\theta_{e,g}) & -sin(\theta_{e,g} - \frac{2\pi}{3}) & -sin(\theta_{e,g} + \frac{2\pi}{3}) \\ \frac{1}{2} & \frac{1}{2} & \frac{1}{2} \end{bmatrix}}_{[T_{dq0}]} \underbrace{\begin{bmatrix} f_a \\ f_b \\ f_c \end{bmatrix}}_{\vec{f}_{abc}} \tag{17}$$

$$\begin{bmatrix} f_a \\ f_b \\ f_c \end{bmatrix} = \underbrace{\begin{bmatrix} cos(\theta_{e,g}) & -sin(\theta_{e,g}) & 1 \\ cos(\theta_{e,g} - \frac{2\pi}{3}) & -sin(\theta_{e,g} - \frac{2\pi}{3}) & 1 \\ cos(\theta_{e,g} + \frac{2\pi}{3}) & -sin(\theta_{e,g} + \frac{2\pi}{3}) & 1 \end{bmatrix}}_{[T_{dq0}]^{-1}} \begin{bmatrix} f_d \\ f_q \\ f_0 \end{bmatrix} \tag{18}$$

As an example, the Park transformation of the first system equation presented in (16) is performed.

$$[\mathbf{L_c}]\frac{d}{dt}\vec{\imath}_{c,abc} + [\mathbf{L_g}]\frac{d}{dt}\vec{\imath}_{g,abc} = \vec{d}_{abc}V_{CC} - \vec{v}_{g,abc} - v_{gc}\vec{u} \tag{19}$$

Thus, by applying (18) to (19) and after that by multiplying the two sides of the equation by (17), the following expression is obtained:

$$\underbrace{[T_{dq0}][\mathbf{L_c}]\frac{d}{dt}[T_{dq0}]^{-1}\vec{\imath}_{c,dq0}}_{\text{1st Term}} + \underbrace{[T_{dq0}][\mathbf{L_g}]\frac{d}{dt}[T_{dq0}]^{-1}\vec{\imath}_{g,dq0}}_{\text{2nd Term}} = \vec{d}_{dq0}V_{CC} - \vec{v}_{g,dq0} - \underbrace{[T_{dq0}]v_{gc}\vec{u}}_{\text{3rd Term}}. \quad (20)$$

When analyzing the 1st Term of (20), it is noted that to solve it, it is necessary to apply the product rule. So,

$$[T_{dq0}][\mathbf{L_c}]\frac{d}{dt}[T_{dq0}]^{-1}\vec{\imath}_{c,dq0} = [T_{dq0}][\mathbf{L_c}]\frac{d}{dt}[T_{dq0}]^{-1}\vec{\imath}_{c,dq0} + \underbrace{[T_{dq0}][\mathbf{L_c}][T_{dq0}]^{-1}}_{[\mathbf{L_c}]}\frac{d}{dt}\vec{\imath}_{c,dq0} \quad (21)$$

Where,

$$[T_{dq0}][\mathbf{L_c}]\frac{d}{dt}[T_{dq0}]^{-1}\vec{\imath}_{c,dq0} = [\mathbf{L_c}]\omega_g\underbrace{\begin{bmatrix}0 & -1 & 0\\ 1 & 0 & 0\\ 0 & 0 & 0\end{bmatrix}\vec{\imath}_{c,dq0}}_{\vec{\imath}_{c,qd}} = [\mathbf{L_c}]\omega_g\vec{\imath}_{c,qd}. \quad (22)$$

$$\vec{\imath}_{c,qd} = [-i_{c,q} \quad i_{c,d} \quad 0]^T \quad (23)$$

In addition, the 2nd Term of (20) is similar to the 1st Term, as described below.

$$[T_{dq0}][\mathbf{L_g}]\frac{d}{dt}[T_{dq0}]^{-1}\vec{\imath}_{g,dq0} = [T_{dq0}][\mathbf{L_g}]\frac{d}{dt}[T_{dq0}]^{-1}\vec{\imath}_{g,dq0} + \underbrace{[T_{dq0}][\mathbf{L_g}][T_{dq0}]^{-1}}_{[\mathbf{L_g}]}\frac{d}{dt}\vec{\imath}_{g,dq0} \quad (24)$$

Where,

$$[T_{dq0}][\mathbf{L_g}]\frac{d}{dt}[T_{dq0}]^{-1}\vec{\imath}_{g,dq0} = [\mathbf{L_g}]\omega_g\underbrace{\begin{bmatrix}0 & -1 & 0\\ 1 & 0 & 0\\ 0 & 0 & 0\end{bmatrix}\vec{\imath}_{g,dq0}}_{\vec{\imath}_{g,qd}} = [\mathbf{L_g}]\omega_g\vec{\imath}_{g,qd}. \quad (25)$$

$$\vec{\imath}_{g,qd} = [-i_{g,q} \quad i_{g,d} \quad 0]^T \quad (26)$$

The 3rd Term of (20) is related to the voltage between the point $v_{n,g}$ and the point $v_{n,c}$. So solving it, we get

$$[T_{dq0}]v_{gc}\vec{u} = v_{gc}\begin{bmatrix}0\\0\\1\end{bmatrix} = v_{gc}\vec{u}_{dq0}. \tag{27}$$

Based on (27), it is noted that the voltage between the points $v_{n,g}$ and $v_{n,c}$ it will only influence the axis component 0. Bearing in mind that the system for connection to the load is three-wire, the voltage $v_{n,g}$ does not interfere in the behavior of the currents injected into the load, since they are currents in a differential mode. Therefore, the voltages v_{gc}, v_{fc} and v_{gf} will be neglected in the modeling. After that, it is possible to rewrite (20) as presented in (28).

$$[\mathbf{L_c}]\frac{d}{dt}\vec{\imath}_{c,dq0} + [\mathbf{L_c}]\omega_g\vec{\imath}_{c,qd} + [\mathbf{L_g}]\frac{d}{dt}\vec{\imath}_{g,dq0} + [\mathbf{L_g}]\omega_g\vec{\imath}_{g,qd} = \vec{d}_{dq0}V_{CC} - \vec{v}_{g,dq0}. \tag{28}$$

As a result, the same transformation methodology can be applied to the other system equations (16). Thus, the system that describes the dynamic behavior of the inverter connected to the load by means of the LCL filter damped in dq0 coordinates is presented in (29).

$$\begin{cases} [\mathbf{L_c}]\frac{d}{dt}\vec{\imath}_{c,dq0} + [\mathbf{L_c}]\omega_g\vec{\imath}_{c,qd} + [\mathbf{L_g}]\frac{d}{dt}\vec{\imath}_{g,dq0} + [\mathbf{L_g}]\omega_g\vec{\imath}_{g,qd} = \vec{d}_{dq0}V_{CC} - \vec{v}_{g,dq0} \\ [\mathbf{L_c}]\frac{d}{dt}\vec{\imath}_{c,dq0} + [\mathbf{L_c}]\omega_g\vec{\imath}_{c,qd} = \vec{d}_{dq0}V_{CC} - \vec{v}_{cf,dq0} \\ [\mathbf{L_g}]\frac{d}{dt}\vec{\imath}_{g,dq0} + [\mathbf{L_g}]\omega_g\vec{\imath}_{g,qd} = \vec{v}_{cf,dq0} - \vec{v}_{g,dq0} \\ [\mathbf{C_d}]\frac{d}{dt}\vec{v}_{cd,dq0} + [\mathbf{C_d}]\omega_g\vec{v}_{cd,qd} = \frac{\vec{v}_{cf,dq0}}{R_d} - \frac{\vec{v}_{cd,dq0}}{R_d} \\ [\mathbf{C_f}]\frac{d}{dt}\vec{v}_{cf,dq0} + [\mathbf{C_f}]\omega_g\vec{v}_{cf,qd} = \vec{\imath}_{c,dq0} - \vec{\imath}_{g,dq0} - \left(\frac{\vec{v}_{cf,dq0}}{R_d} - \frac{\vec{v}_{cd,dq0}}{R_d}\right) \end{cases} \tag{29}$$

Where,

- $\vec{v}_{g,dq0}$: is the load phase voltages vector in dq0 coordinates;
- $\vec{\imath}_{c,dq0}$: is the output phase currents vector in dq0 coordinates;
- $\vec{\imath}_{g,dq0}$: is the load injected phase currents vector in dq0 coordinates;

• $\vec{v}_{cf,dq0}$: is the voltage vector of the LCL filter capacitors connected in the abc phases in dq0 coordinates;

• $\vec{v}_{cd,dq0}$: is the vector of the voltages of the capacitors of the damping branch connected in the abc phases in dq0 coordinates;

• $\vec{d}_{dq0}$: is the duty cycles inverter vector in dq0 coordinates;

• ω_g: is the load voltage fundamental frequency in rad/s;

3.1.2 Decoupling the Axes (*dq*)

Note that the mathematical modeling using the Park transform inserts a coupling between the d and q axes. As the order of the modeled system is increased, the number of couplings is also proportionally increased. In order to make the model linear to apply in the design of current controllers, a mathematical method of decoupling between the axes must be used.

The decoupling method adopted to solve this problem is based on [40], where it is performed for passive filters of the LCL type with damping. Therefore, the decoupling related to the inductances L_c and L_g for the d axis is described by (30) and (31).

$$\mathbf{d}L_c = \omega_g L_c i_{c,q} \tag{30}$$

$$\mathbf{d}L_g = \omega_g L_g i_{c,q} \tag{31}$$

It is important to note that (31) is a simplification considering that the current $i_{g,d}$ corresponds to the almost instantaneous average value of the current $i_{c,d}$, so it is possible to use this method to perform the decoupling related to inductance L_g. The decoupling of capacitors C_f and C_d can be performed by applying the same procedure, as described below [37].

$$\mathbf{d}C_f = \omega_g L_c \cdot s(C_f v_{cf,q}) \tag{32}$$

$$\mathbf{d}C_d = \omega_g L_c \cdot s(C_d v_{cd,q}) \tag{33}$$

After that, the total decoupling factor for the d axis and q axis is represented by (34) and (35).

$$\mathbf{d}LCL = \mathbf{d}L_c + \mathbf{d}L_g + \mathbf{d}C_f + \mathbf{d}C_d = \omega_g(L_c + L_g)i_{c,q} + \omega_g L_c \cdot s(C_f v_{cf,q} + C_d v_{cd,q}) \quad (34)$$

$$\mathbf{q}LCL = -\omega_g(L_c + L_g)i_{c,d} - \omega_g L_c \cdot s(C_f v_{cf,d} + C_d v_{cd,d}) \quad (35)$$

Decoupling can be performed by introducing feedforward compensation components to represent the terms inherent to the coupling [40]. In addition, it is noted that the decoupling of the inductances is easily accomplished using the almost instantaneous average value of the currents $i_{c,dq}$, or $i_{g,dq}$. However, the decoupling of the capacitors depends on the derivative of their voltages, as described by (32) and (33). Considering that the dynamics of current controllers are predominantly dependent on the L_c and L_g inductances and that the capacitors have little influence on the cutoff frequency of the control strategy, as the current flowing through the capacitors is basically multiple frequencies of the switching and low frequency amplitude [40]. The coupling between the capacitors will be neglected, considering that the current controllers are able to reject these disturbances. Thus, a new duty cycle is defined to perform the decoupling between the axes d and q referred to in the inductances L_c and L_g, as described in (36).

$$\begin{cases} d'_d = d_d + \left(\frac{\mathbf{d}L_c + \mathbf{d}L_g}{V_{CC}}\right) = d_d + \frac{\omega_g(L_c+L_g)i_{c,q}}{V_{CC}} \\ d'_q = d_q - \left(\frac{\mathbf{q}L_c + \mathbf{q}L_g}{V_{CC}}\right) = d_q - \frac{\omega_g(L_c+L_g)i_{c,d}}{V_{CC}} \end{cases} \quad (36)$$

Isolating d_d and d_q in (36) and applying in (29), we obtain the system of equations that governs the dynamic behavior of the inverter connected to the mains through the damped LCL filter mathematically decoupled, as

$$\begin{cases} [\mathbf{L_c}]\frac{d}{dt}\vec{\imath}_{c,dq0} + [\mathbf{L_g}]\frac{d}{dt}\vec{\imath}_{g,dq0} += \vec{d}_{dq0}V_{CC} - \vec{v}_{g,dq0} \\ [\mathbf{L_c}]\frac{d}{dt}\vec{\imath}_{c,dq0} = \vec{d}_{dq0}V_{CC} - \vec{v}_{cf,dq0} \\ [\mathbf{L_g}]\frac{d}{dt}\vec{\imath}_{g,dq0} = \vec{v}_{cf,dq0} - \vec{v}_{g,dq0} \\ [\mathbf{C_d}]\frac{d}{dt}\vec{v}_{cd,dq0} = \frac{\vec{v}_{cf,dq0}}{R_d} - \frac{\vec{v}_{cd,dq0}}{R_d} \\ [\mathbf{C_f}]\frac{d}{dt}\vec{v}_{cf,dq0} = \vec{\imath}_{c,dq0} - \vec{\imath}_{g,dq0} - \left(\frac{\vec{v}_{cf,dq0}}{R_d} - \frac{\vec{v}_{cd,dq0}}{R_d}\right) \end{cases} \quad (37)$$

3.1.3 Current Control Oriented Modeling

In larger order systems, the state space method is widely used in the literature, because based on matrices of inputs, outputs and states of the system it is possible to obtain the transfer functions necessary for the design of current controllers [36]. Thus, the format of the state space method is described by (38).

$$\begin{cases} \dot{x}(t) = \mathbf{A}x(t) + \mathbf{B}u(t) \\ (t) = \mathbf{C}x(t) + \mathbf{E}u(t) \end{cases} \tag{38}$$

Where A is called the state matrix, B the input matrix, C the output matrix and D the feedforward matrix. Figure 6 illustrates the block diagram that represents the state space method described by (38). The state variables, the inputs and outputs of the system are defined in (39), (40) and (41), respectively. In addition, it was considered that the voltage in the load is constant towards the switching frequency of the inverter, therefore $\vec{v}_{g,dq0}$=0.

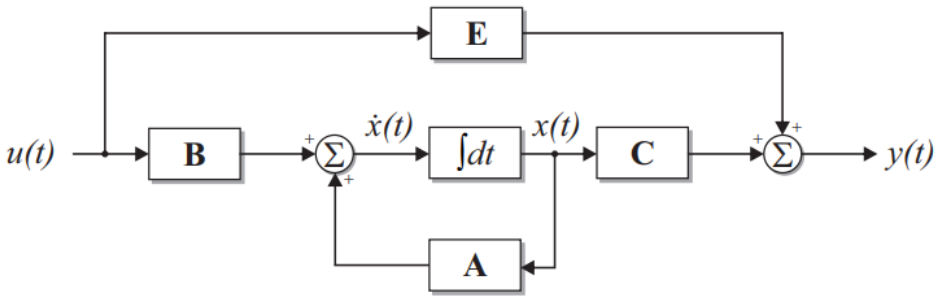

Figure 6 Block diagram of the state space method [36]

Where:

$$y = [\hat{\imath}_{c,d} \quad \hat{\imath}_{g,d} \quad \hat{\imath}_{c,q} \quad \hat{\imath}_{g,q}]^T \tag{39}$$

$$x = [\hat{\imath}_{c,d} \quad \hat{\imath}_{g,d} \quad \hat{v}_{cf,d} \quad \hat{v}_{cd,d} \quad \hat{\imath}_{c,q} \quad \hat{\imath}_{g,q} \quad \hat{v}_{cf,q} \quad \hat{v}_{cd,q}]^T \tag{40}$$

$$u = [\hat{d}'_d \quad \hat{d}'_q]^T \tag{41}$$

In addition, matrices A, B and C are represented as follows,

$$\mathbf{A} = \begin{bmatrix} 0 & 0 & \frac{-1}{L_c} & 0 & 0 & 0 & 0 & 0 \\ 0 & 0 & \frac{1}{L_g} & 0 & 0 & 0 & 0 & 0 \\ \frac{1}{C_f} & \frac{-1}{C_f} & \frac{-1}{R_d C_f} & \frac{1}{R_d C_f} & 0 & 0 & 0 & 0 \\ 0 & 0 & \frac{1}{R_d C_d} & \frac{-1}{R_d C_d} & 0 & 0 & 0 & 0 \\ 0 & 0 & 0 & 0 & 0 & 0 & \frac{-1}{L_c} & 0 \\ 0 & 0 & 0 & 0 & 0 & 0 & \frac{1}{L_g} & 0 \\ 0 & 0 & 0 & 0 & \frac{1}{C_f} & \frac{-1}{C_f} & \frac{-1}{R_d C_f} & \frac{1}{R_d C_f} \\ 0 & 0 & 0 & 0 & 0 & 0 & \frac{1}{R_d C_d} & \frac{-1}{R_d C_d} \end{bmatrix} \quad (42)$$

$$\mathbf{B} = \begin{bmatrix} \frac{V_{CC}}{L_c} & 0 \\ 0 & 0 \\ 0 & 0 \\ 0 & 0 \\ 0 & \frac{V_{CC}}{L_c} \\ 0 & 0 \\ 0 & 0 \\ 0 & 0 \end{bmatrix} \quad (43)$$

$$\mathbf{C} = \begin{bmatrix} 1 & 0 & 0 & 0 & 0 & 0 & 0 & 0 \\ 0 & 1 & 0 & 0 & 0 & 0 & 0 & 0 \\ 0 & 0 & 0 & 0 & 1 & 0 & 0 & 0 \\ 0 & 0 & 0 & 0 & 0 & 1 & 0 & 0 \end{bmatrix} \quad (44)$$

Thus, from (38) it is possible to obtain the transfer functions by applying the Laplace transform and performing a mathematical manipulation as described in (45).

$$\mathbf{G}(s) = \frac{y(s)}{u(s)} = \mathbf{C}(s\mathbf{I} - \mathbf{A})^{-1}\mathbf{B} + \mathbf{D} \quad (45)$$

Where I is an identity matrix resulting from the mathematical manipulation performed. In addition, it is worth mentioning that the matrix D, in (45), is null, considering that no feedforward is considered in the modeling. Thus, by means of (45) a matrix of dimension 4x2 is obtained, as shown below.

$$\mathbf{G}(s) = \frac{y(s)}{u(s)} = \mathbf{C}(s\mathbf{I} - \mathbf{A})^{-1}\mathbf{B} = \begin{bmatrix} \frac{\hat{\imath}_{c,d}}{\hat{d}'_d} & \frac{\hat{\imath}_{c,d}}{\hat{d}'_q} \\ \frac{\hat{\imath}_{g,d}}{\hat{d}'_d} & \frac{\hat{\imath}_{g,d}}{\hat{d}'_q} \\ \frac{\hat{\imath}_{c,q}}{\hat{d}'_d} & \frac{\hat{\imath}_{c,q}}{\hat{d}'_q} \\ \frac{\hat{\imath}_{g,q}}{\hat{d}'_d} & \frac{\hat{\imath}_{g,q}}{\hat{d}'_q} \end{bmatrix} \tag{46}$$

Note that the transfer functions obtained were from the system currents with respect to the duty cycles of the inverter in dq coordinates. The first column describes the current transfer functions with respect to the d-axis duty cycle, as well as in the second column it relates to the q-axis duty cycle. However, it is worth noting that the currents on the d axis cannot be influenced by the duty cycle of the q axis, due to the mathematical decoupling previously developed. Thus, these transfer functions must be null, and the opposite is also true, that is, q-axis currents are not influenced by the d-axis duty cycle. That said, the respective transfer functions are described by (47) and (48).

$$\frac{\hat{\imath}_{c,dq}}{\hat{d}'_{dq}} = \frac{V_{CC}[C_d C_f L_c R_d s^3 + (C_d + C_f) L_g s^2 + C_d R_d s + 1]}{[C_d C_f L_c L_g R_d s^4 + (C_d + C_f) L_c L_g s^3 + (L_c + L_g) C_d R_d s^2 + (L_c + L_g) s]} \tag{47}$$

$$\frac{\hat{\imath}_{g,dq}}{\hat{d}'_{dq}} = \frac{V_{CC}[C_d R_d s + 1]}{[C_d C_f L_c L_g R_d s^4 + (C_d + C_f) L_c L_g s^3 + (L_c + L_g) C_d R_d s^2 + (L_c + L_g) s]} \tag{48}$$

When checking the transfer functions (47) and (48), the dependence with respect to some parameters is observed, such as DC bus voltage, inductors and capacitors of the LCL filter, among others. Therefore, Table 3 presents the parameters used for the design of the current controllers.

Table 3 Parameters of the 2L Inverter and LCL filter.

Variable Parameter Specifications	**Variable Parameter Specifications**	**Variable Parameter Specifications**
Active Power	P_{grid}	1,5 kW

Effective Line Voltage at Load	$V_{ll,abc}$	400 V
Load frequency	f_{load}	50 Hz
Inverter Switching Frequency	f_{si}	10 kHz
Inverter Output Effective Current	$I_{g,abc}$	11,34 A
DC Bus Voltage	V_{CC}	120 V
Current Ripple	$\Delta i_{c,max}$	20%
Ratio Factor of Capacitors C_f and C_d	α_C	1
Relation Factor of Inductances $L_c$and L_g	α_L	1
Filter Capacitor	C_f	27,5 μF
Passive Damping Capacitor	C_d	27,5 μF
Inverter Side Inductor	L_c	293 μH
Load Side Inductor	L_g	293 μH
Passive Damping Resistor	R_d	3 Ω
Filter Resonance Frequency	f_{res}	2500 Hz

3.1.4 Current Controller Design

Once the transfer functions are defined, the next step is to design the current controller. Therefore, the control system of the currents injected into the load is presented in the block diagram as shown in Figure 7. In order to simplify the analysis for the design of the controllers, current control was based on [36].

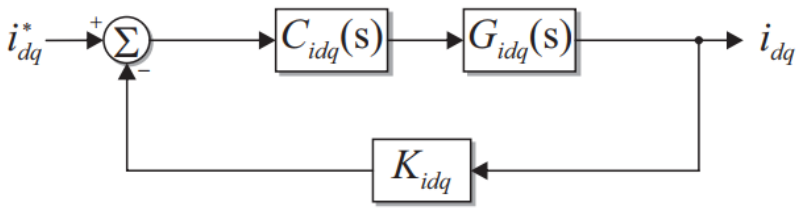

Figure 7 Block diagram for the control of currents in the load [36].

From Figure 7, $G_{idq}(s)$ represents the transfer functions obtained in (47) and (48) that relate the currents injected into the load with the cyclical ratios of the inverter. The current sensor gain K_{idq} was considered unitary, given that it can be compensated via software, thus making it possible to monitor and control the system in relation to its real operating values. The great advantage of controlling the currents in the plane *dq0* is the fact that sinusoidal quantities, with frequency equal to the fundamental frequencies, are seen as constant signals over time. Therefore, it is possible by using Proportional-Integral (PI) controllers to guarantee zero error in a steady state for sinusoidal signals at the fundamental frequency. Thus, the PI controller is described by (49).

$$C_{idq}(s) = K_{ci}\left(\frac{s+\omega_{zi}}{s}\right) \tag{49}$$

Since all the blocks in the diagram in Figure 7 have been described, it is possible to design the current controllers using the frequency response method. In view of the above, the analysis begins with the non-compensated open-loop transfer function. For this, the multiplication is performed between all blocks, except the controller $C_{idq}(s)$, according to (50).

$$OLTF(s) = G_{idq}(s)K_{idq} \tag{50}$$

When analyzing (50), it appears that the transfer function does not have poles at the origin, therefore, no null error is obtained in a steady state. Using the PI controller (49) in (50), the compensated open loop transfer function is obtained, as

$$OLTF_{Ci}(s) = \underbrace{K_{ci}\left(\frac{s+\omega_{zi}}{s}\right)}_{C_{idq}(s)} OLTF_{NCi}(s). \tag{51}$$

From this definition, one can determine the $OLTF_{Ci}(s)$ in sinusoidal steady state, where $s = j\omega$. So,

$$OLTF_{Ci}(j\omega) = \underbrace{K_{ci}\left(\frac{j\omega+\omega_{zi}}{j\omega}\right)}_{C_{idq}(j\omega)} OLTF_{NCi}(j\omega). \tag{52}$$

Thus, using the module condition and the phase margin concept, determined by (53) and (54), respectively, we obtain (55) and (56), which allows the calculation of the frequency values ω_{zi} and gain K_{ci}.

$$|OLTF_{Ci}(\omega)||_{\omega=\omega_{ci}} = 1 \tag{53}$$

$$PM = 180° + \angle OLTF_{Ci}(\omega)|_{\omega=\omega_{ci}} \tag{54}$$

$$\omega_{zi} = \frac{\omega_{ci}}{tg[PM-90°-\angle OLTF_{NCi}(\omega_{ci})]} \tag{55}$$

$$K_{ci} = \frac{\omega_{ci}}{(\sqrt{\omega_{ci}^2+\omega_{zi}^2})|OLTF_{NCi}(\omega_{ci})|} \tag{56}$$

Figure 8 shows the Bode diagram of the transfer function (48) and also without passive damping, that is, R_d=0 e C_d=0.

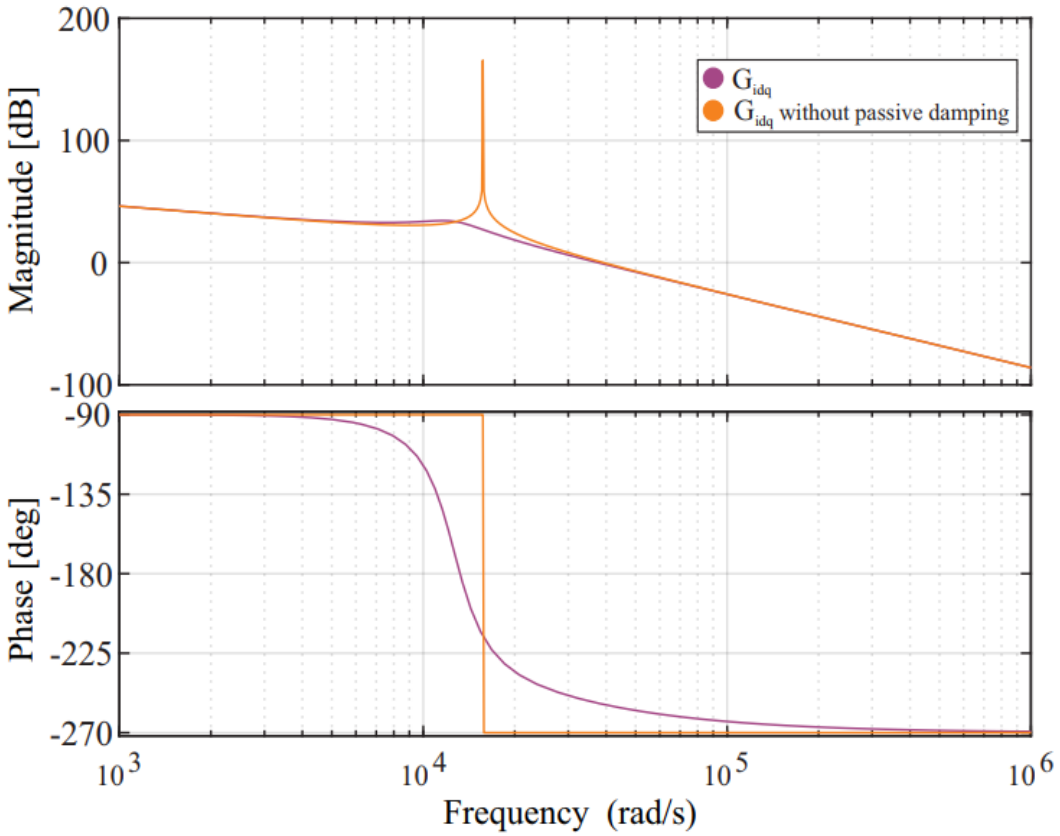

Figure 8 Bode diagram of the current model

From Figure 8, it is possible to verify the peak caused by the resonance frequency of the LCL filter, at 2500 Hz (approximately 15.7 krad/s). The peak caused by the resonance is attenuated using passive damping on the filter, which is composed of the RC branch (see Figure 5). In addition, the current model transfer function has a crossing frequency of 6366 Hz. It is noted that in the resonance frequency there is an inversion of 180º in the phase before crossing by zero, thus requiring a current control. In addition, analyzing the system bandwidth, the following frequencies were verified: switching frequency of the inverter f_{si} =10 kHz and resonance frequency of the LCL filter f_{res}=2500 Hz. Thus, the design parameters for the current controllers were realized by allocating the phase margin at PM=60 ° and the crossing frequency at f_{ci}=250 Hz (ω_{ci}=1571 rad/s). Thus, applying these design parameters in (55) and (56), we obtain:

$$K_{ci} = 0{,}0046 \tag{57}$$

$$\omega_{zi} = 465\text{rad/s} \tag{58}$$

$$C_{ix}(s) = 0{,}0046\left(\frac{s+465}{s}\right) \tag{59}$$

Figure 9 presents the Bode diagram of the open-loop and closed-loop compensated transfer functions.

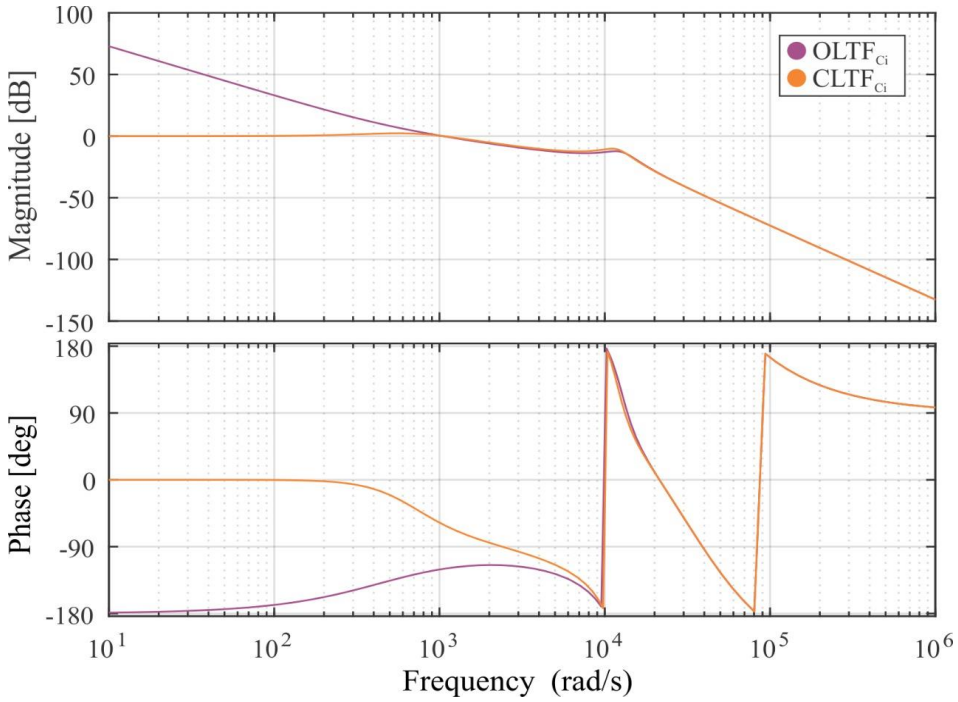

Figure 9 Bode diagram open-loop and closed-loop compensated tranfer functions.

Note that the PI controller design specifications were met, crossing frequency 250 Hz and phase margin 60º, as well as a gain margin of 10.5 dB, which guarantees a good attenuation of the PI controller for frequencies greater than f_{ci}.

3.1.5 Droop Control: Modeling And Implementation

As previously presented, the droop control is a strategy commonly used in connected and isolated inverters, since it allows a contribution of the generation in the control of voltage and output frequency, both for inverters connected to the grid operating as grid following, and grid forming where they are able to determine the behavior of the grid, or even feed isolated loads. The basis for the implementation and modeling of the droop control in this work, was based on [41], which presents different implementations: grid following, also called Current Control

Mode (CCM), and grid forming, also called Voltage control mode (VCM). In our case, for the purposes of simulation and modeling, the concept of grid forming inverter (VCM) was used, where the inverter must control the voltage and frequency in the output load. Figure 10 shows the working methodology of the inverter with VCM droop control.

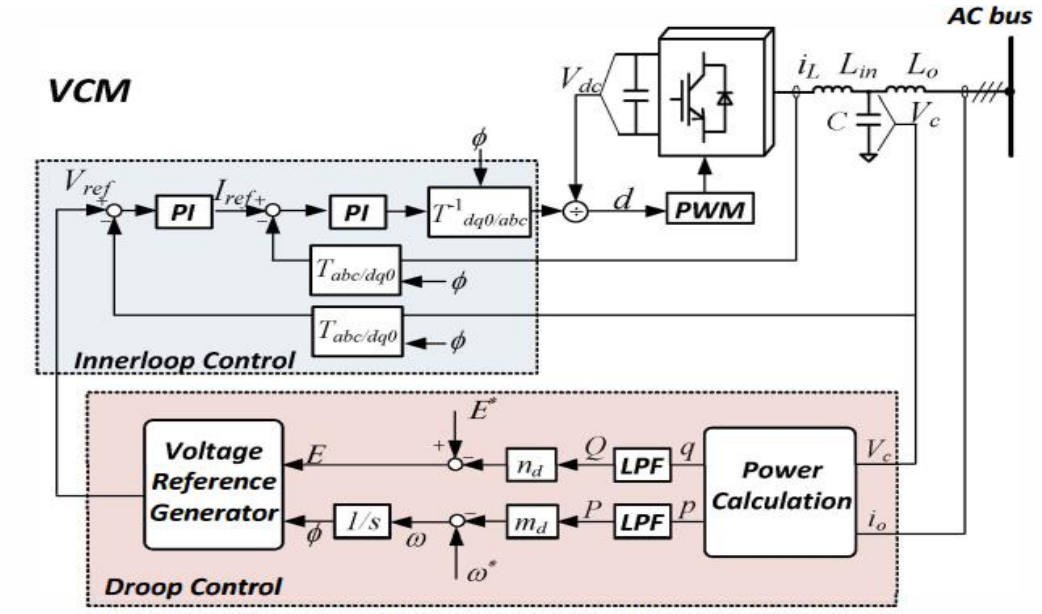

Figure 10 Inverter operating with VCM droop control [41].

In Figure 10 above, the generic methodology of the network-forming droop control is presented. The droop control loop is initially composed of the "**Power Calculation**" block, which is responsible for receiving the measurements of the inverter output (voltage and current), and calculating the power that is being delivered at the output, and with that, through a low-pass filter, calculate an additional portion of reference voltage and frequency that adds up to the already known reference voltage and frequency. Instantaneous active and reactive powers are calculated according to the instantaneous power theory:

$$p = v_{cd} i_{od} + v_{cq} i_{oq} \tag{60}$$

$$q = v_{cq} i_{od} - v_{cqd} i_{oq} \tag{61}$$

Where p and q are the output powers of the inverter that flow to the AC bus, v_{cd} and v_{cq} are the measurable output voltages, and i_{od} and i_{oq} are the output currents, all in dq coordinates.

The droop coefficients m_d and m_q are designed to meet the specifications for maximum output variation:

$$m_d = \frac{\Delta\omega}{P_{max}} \tag{62}$$

$$m_q = \frac{\Delta E}{Q_{max}} \tag{63}$$

Where $\Delta\omega$ and ΔE are the maximum desired variations in frequency and voltage at the output. For the design of these gains in this work, it was considered 5% of maximum frequency variation and 10% of voltage drop/raise, for the maximum variation of load. The low pass filter can be implemented or not depending on the application, more details can be seen in [41]. The design parameters are presented in the Appendix. To operate as grid forming, the inverter has a "**Voltage Reference Generator**", which generates the voltage reference according to the droop output plus the fixed voltage and frequency references (E^* and ω). Also, the speed reference goes through an integrator, to generate the angle reference Φ for the sinusoidal voltage, which is transformed into dq coordinates. With the error between this reference voltage and the measured output voltage, a PI controller is added in order to reset the voltage error, resulting in a reference current I_{ref}. Again, the error between the reference current and the inverter output current is processed and passes through a PI, in order to reset this error. The output is a control signal transformed into a duty ratio that controls the inverter switches via the PWM signal. Obviously, between the measurament stage and processing a transformation between abc and dq coordinates is needed. This steps are not detailed in this work, but references can be found in [36]. The voltage and current measurements at the inverter output can be obtained from the filter capacitor and inductors, respectively, as shown in the Figure 10, or they can be measured at another output point, such as the load, for example.

3.2 Parallel Inverters Operation

Obviously, the operation of inverters in parallel increases the power supply capacity. In addition, the system tends to become more reliable in energy supply. On the other hand, parallel operation brings some challenges, due to the need for synchronization between the inverters. Poor parallel operation of inverters can cause instability [42]. Figure 11 shows an example of

parallel operation of inverters, with line impedance Z_{line1} and Z_{line2}. The inverters can be connected to the same DC bus, or have the individual DC bus.

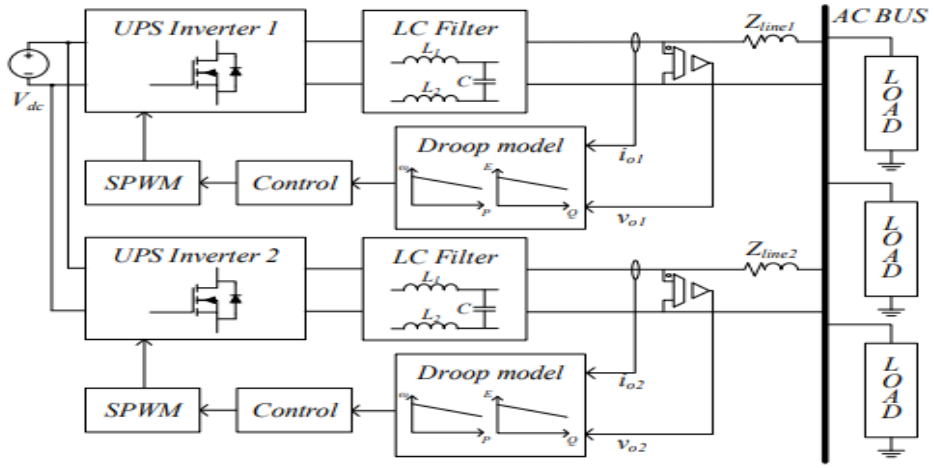

Figure 11 Parallel operation of inverters [43]

The operation is generally divided into centralized control, master-slave control, decentralized control based on communication lines. In addition, the droop control strategy is widespread and well-regarded, as it does not need lines and communication signals between the inverters. Therefore, for inverter operation in parallel, mainly in isolated operation, the droop control strategy is capable of operation with satisfactory performance [44]. In this context, droop control is applied to the two inverters for the operation in parallel feeding isolated load in this work.

4 RESULTS AND ANALYSIS

In this chapter, the results obtained in simulations and analyses will be presented, based on the methodologies presented in the previous sections. Section 4.1 presents the results of nonlinear simulation for an inverter operation feeding a separate load operating as grid forming and the state space modeling for this case. Section 4.2 presents the results of the parallel operation of two identical inverters feeding an isolated load, also operating in grid forming mode, in addition the state space modeling of the parallel system. For simulations, the Simulink toolbox of the MATLAB was used.

4.1 Results for the Inverter Operation Feeding Isolated Load

The simulation for this system is presented in Figure 12.

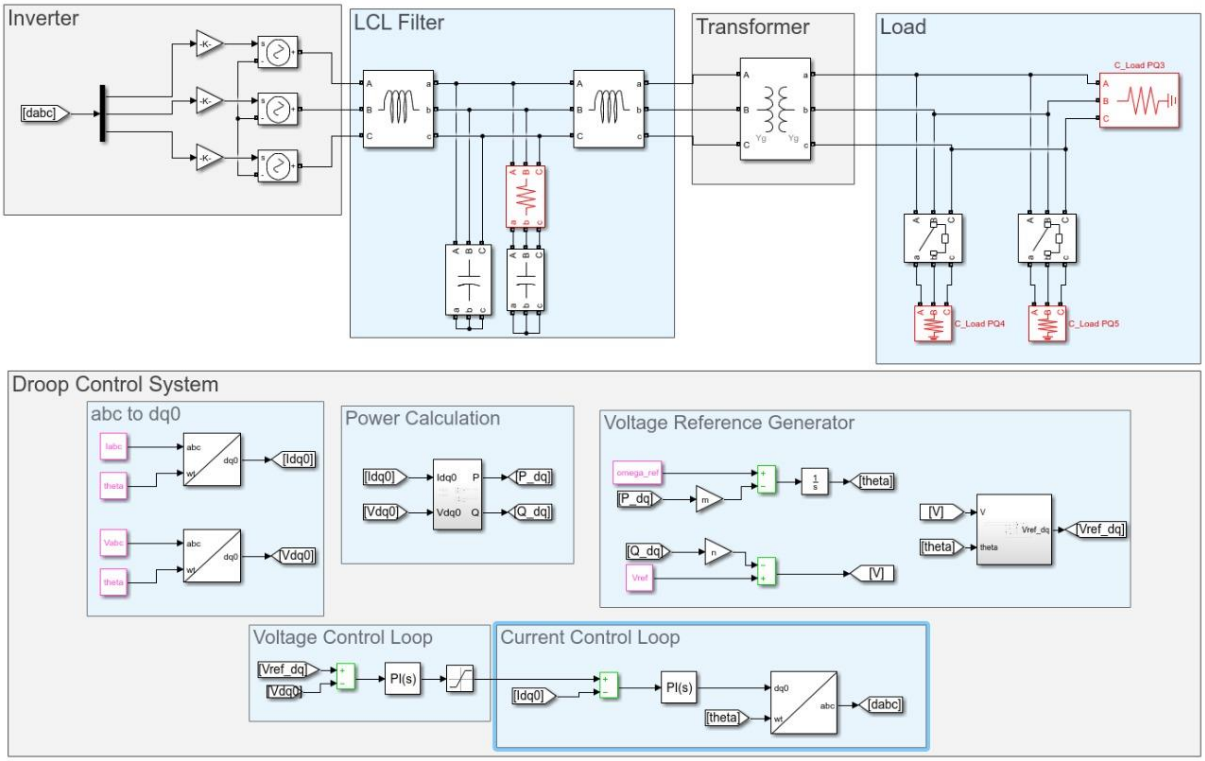

Figure 12 Inverter feeding an isolated load.

As discussed and modeled in the previous sections, the inverter was simulated using the average model, and the parameters of the inverter + filter set are generated in Table 3. The load was modeled as active, ignoring the reactive effect, since for the analysis in question this would not have much influence. Still 3 scenarios were considered as described below:

- **Scenario 1:** The system starts with a load of 1 kW, and after 1 second, a load of 500 W is switched, reaching the nominal power of the inverter, and at t = 2s, the load of 500 W is removed, returning to operation with 1 kW.
- **Scenario 2**: The system starts with a load of 200W, and at t = 1s, a load of 1300 W is switched, reaching the nominal power of the inverter, and at t = 2s, the load of 1300 W is removed, returning to operation with load of 200W.
- **Scenario 3**: Scenario 3 is the most critical scenario. To test the current limitation (and consequently the inverter's output power), the inverter is subjected to a load

greater than its nominal power, testing the current limitation imposed on the inverter through a saturator in voltage control loop output (limiting the reference current). The system starts with a load of 200 W, and after 1 second, a 1300 W load is switched, reaching the nominal power of the inverter (1.5kW), and at t = 2s, a load of 1 kW is added, totaling a load of 2.5 kW (166% of the nominal power of the inverter).

The scenarios were chosen in order to test the operation of the droop control, both in the cases injection of more power (load increase) as well as in the injection of less power (load decrease), in order to control voltage and output frequency in the load. In addition, a saturator was added to current control input, for scenarios where the load exceeds the maximum allowed by the inverter, in order to avoid possible instability.

4.1.1 Scenario 1

For Scenario 1, Figure 13 and Figure 14 show the inverter and load output power, and the load current, respectively. Because the system is balanced, the sinusoidal line current in one phase is shown only.

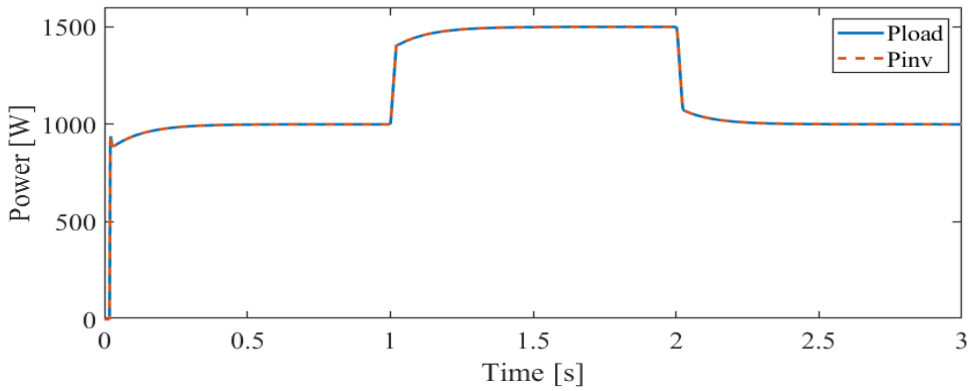

Figure 13 Output power and load power.

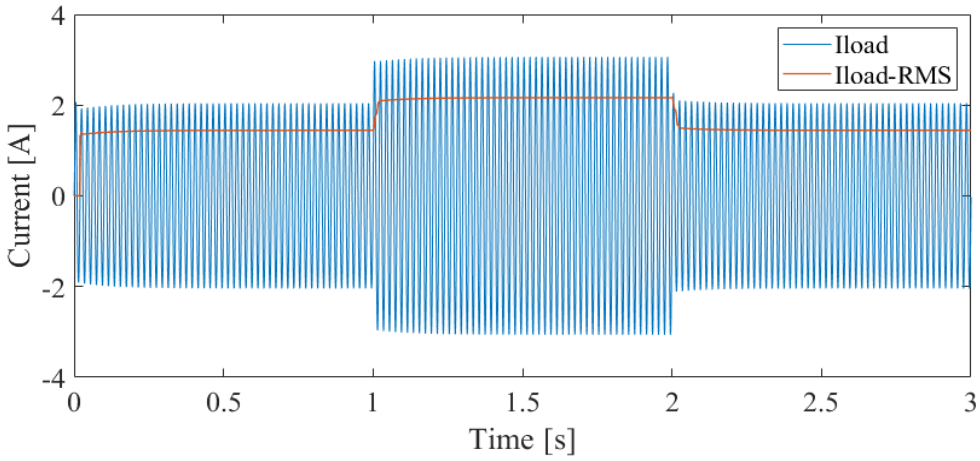

Figure 14 Load Current (Line and RMS).

Although the loading steps are small, the inverter quickly responds to the rise and fall of load, at 1s and 2s respectively. The speed of this control depends mainly on the current control loops. Furthermore, as transmission losses are not being considered, as the inverter is very close to the load, the output power of the inverter is practically the power supplied to the load. Figure 15 and Figure 16 show the load frequency and voltage. Because the system is balanced, the sinusoidal line voltage between phases a and b is shown only.

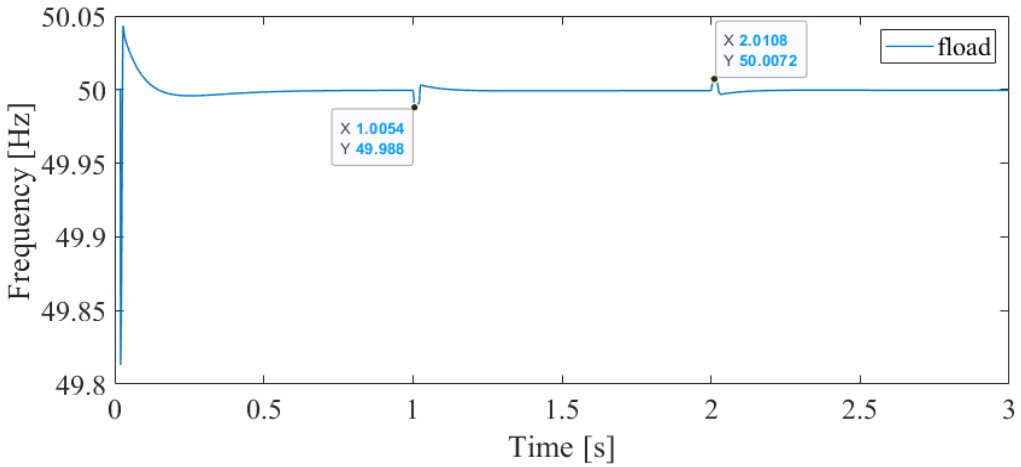

Figure 15 Load frequency.

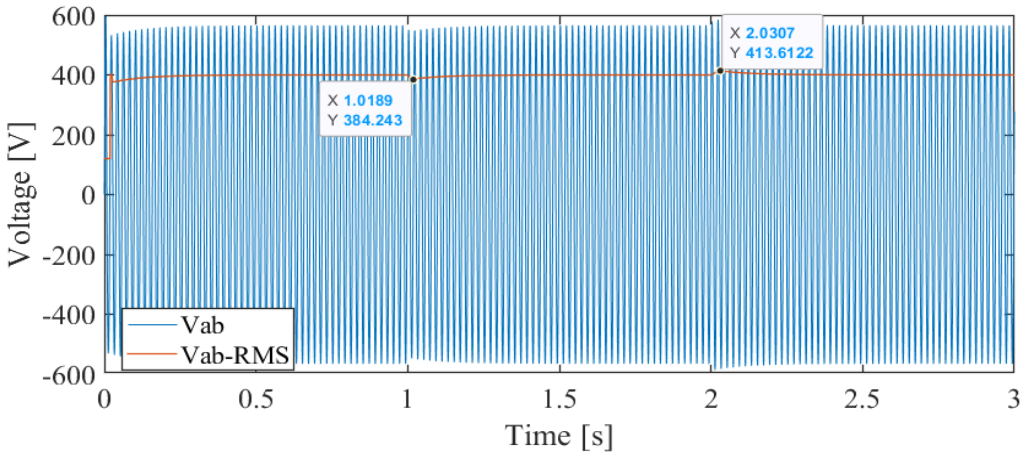

Figure 16 Load Voltage (Line and RMS).

Through the voltage and frequency graphs it is possible to see that the implemented droop control satisfactorily meets the requirements. On the load steps that the inverter is subjected to, the control is able to bring the voltage and frequency back to very close to their nominal values. In this case, from a load step of 50% of the inverter's capacity, the frequency reached a minimum value of 49.988, and a voltage drop to about 384 V_{rms}, respecting the design specifications.

4.1.2 Scenario 2

The results for Scenario 2, show the work of droop loops more prominently. This is because the load variations are sudden, reaching almost 100% of the nominal power of the inverter. This means that the inverter control needs to act more aggressively to avoid voltage and frequency deviations. Figure 17 and Figure 18 show the output power and load power, and load current,

respectively.

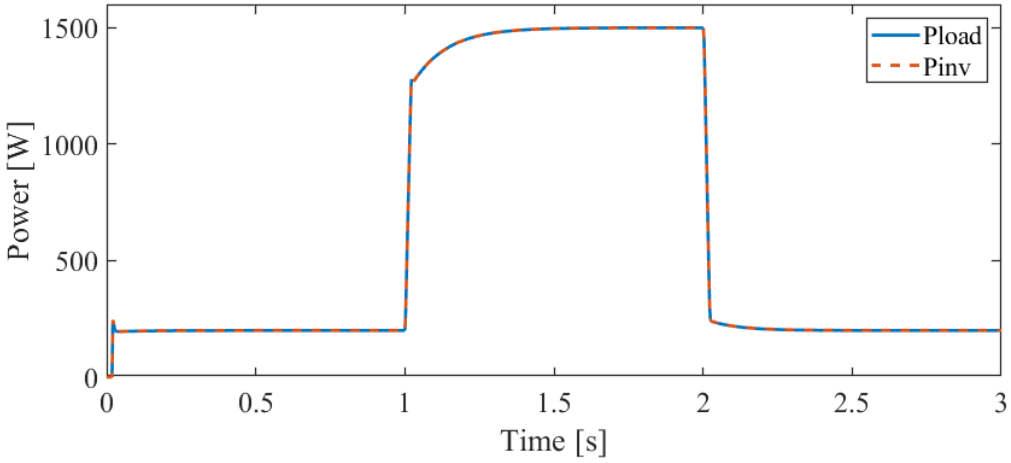

Figure 17 Output Power and Load Power.

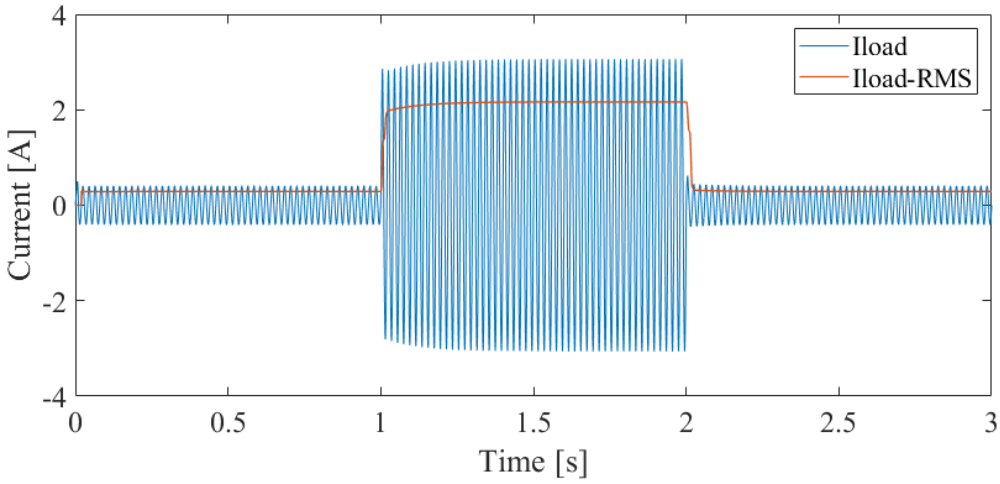

Figure 18 Load Current (Line and RMS).

Despite the more aggressive dynamics, the inverter is able to quickly increase the output power to supply the load at t = 1s. The same can be seen in the opposite case, that is, when the load drops from 1.5 kW to 200 W. Figure 19 and Figure 20 present the frequency and load voltage for this scenario.

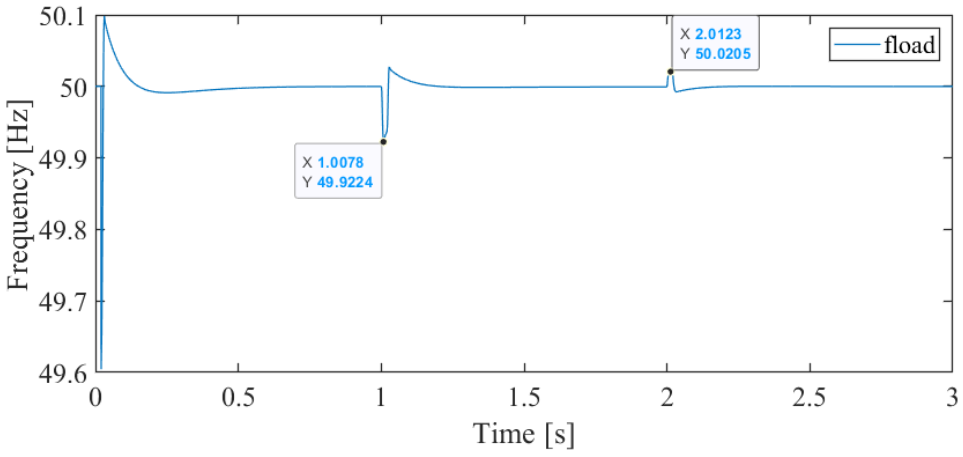

Figure 19 Load Frequency.

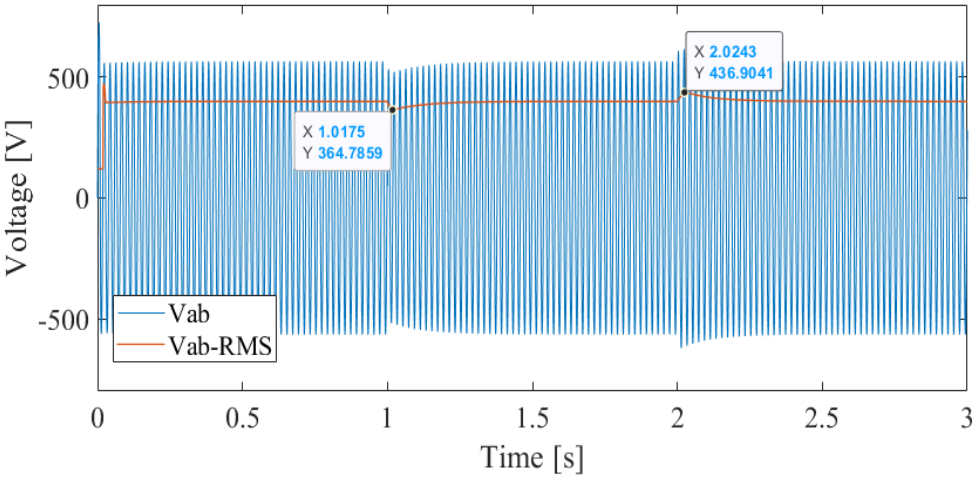

Figure 20 Load Voltage (Line and RMS).

Following the same analysis, for this scenario, which was purposely a much more critical variation, the frequency reaches 49.9224 Hz, which characterizes a drop of 0.15%, respecting the design limits. Looking at the voltage drop when there is a load step (t = 1s), there is a more significant drop to 364.7859 V_{rms}, which characterizes 9.6% of the nominal RMS voltage (400 V) value, which still meets the specifications of the droop control.

4.1.3 Scenario 3

For Scenario 3, the load exceeding the inverter's nominal power was chosen to test the inverter control limits, as discussed in the description of the scenarios. For this, Figure 21, Figure 22,

Figure 23 and Figure 24 respectively show: the inverter output power and load power, the load current, the frequency, and voltage.

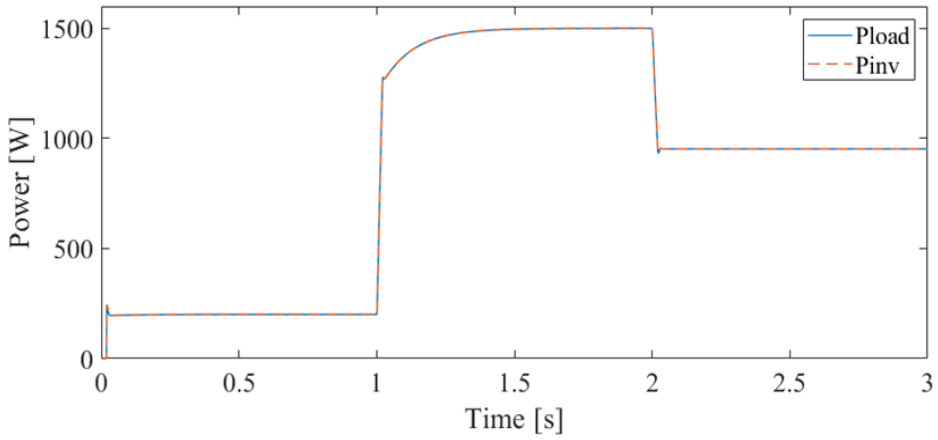

Figure 21 Output Power and Load Power

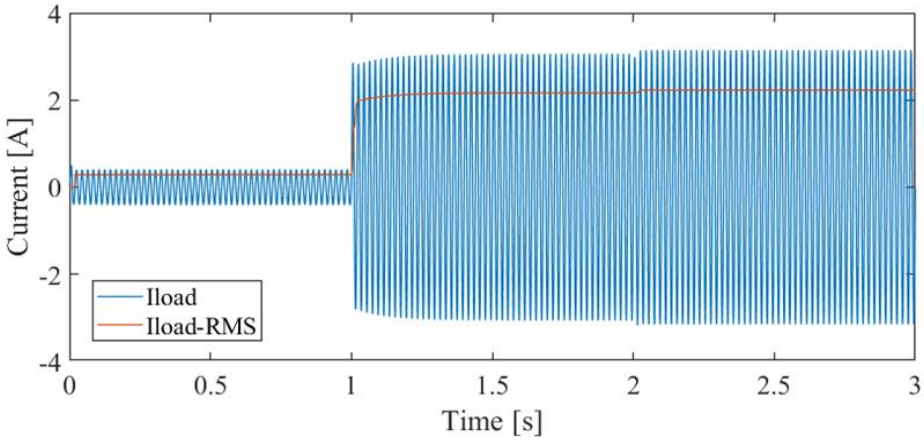

Figure 22 Load Current (Line and RMS)

The load switching that takes place at t = 1s is the repetition of scenario 2, just to get the inverter to stop operating at its maximum power. What interests us in this scenario is the switching at t = 2s, where the load increases to 2.5 kW, which represents 166% of the inverter's nominal capacity. Without the action of limiters in the control loops, the system would have to have some way of recognizing the overpower required, such as a load shedding algorithm. For example, so as not to tend to instability, which can cause severe problems in the operation. To

avoid this, a saturator was implemented in the voltage loop output, so the inverter limits the output current, and consequently limits the output power, causing the load to be feed only partially. This can be clearly seen in Figure 22, where the current hardly changes significantly, since it was already operating at the nominal current.

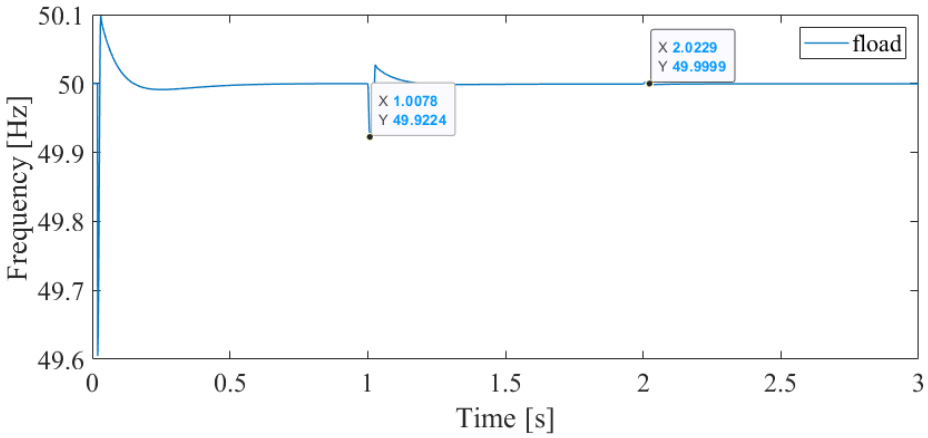

Figure 23 Load Frequency

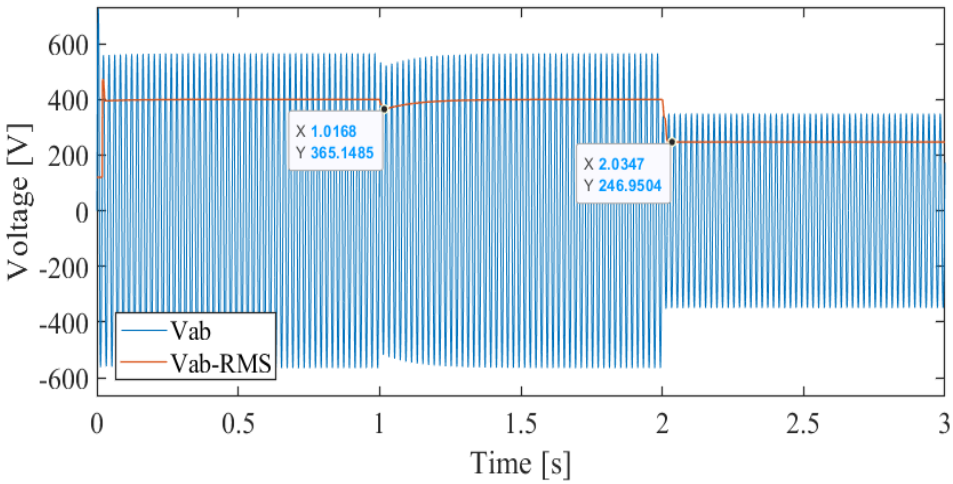

Figure 24 Load Voltage (Line and RMS)

In Figure 24, the voltage drops to around 247 $Vrms$. This happens when the load demands more power than the inverter capacity. The current loop is the most internal of the inverter's hierarchical control, so when the reference current is limited, somehow the power balance must be maintained, because the current loop only adjusts the output current to the reference current, therefore, the inverter will suffer from the voltage delivered to the load. Because the load power

drops along with the output inverter power, there is no significant variation in frequency. So, it acts like a load drop.

4.1.4 State Space Model

In this section, the inverter's state space model is presented. The methodology and equations are the same as shown in Chapter 3. Starting from Equations (42), (43) and (44), having the current and voltage controller designed, the droop control methodology, equations, and parameters shown, it is possible to deduce the state space model of the system as a whole. This model is usually obtained only for inverter + output filter, since it is the structure considered to be more "fixed" in the system as a whole. But what interests us is to find a generic model of the system, which allows us to make linear analyses on the stability of the system. To do this, it is necessary to incorporate the current, voltage and droop controller into the model matrices found in Chapter 3. Therefore, Equations (60), (61), (62) and (63) are incorporated in modeling. It is important to highlight that for the modeling, time delays related to the digital control of the inverter were considered. These delays depend on the sampling period of the system. The procedure for the construction of the linearized matrices was implemented in an algorithm in MATLAB, and its logic is described below:

i. Declaration of the equations obtained from the modeling of each block in the system.
ii. Definition of state variables, inputs, and outputs of the system.
iii. Calculation of the solution and Jacobian matrix to find the equations.
iv. Numerical definition of the values of the variables involved.
v. Calculation of numerical matrices for the operating point.

Details such as: definition of state variables, inputs, processes, as well as generic matrices, are presented in the Appendix, due to the large number of equations, and the large dimension of the matrices, resulting in a 14-order system. These matrices modeled generically are understood as a significant contribution of the work, opening the possibility of changing parameters of the controllers, filters, as well as changing inputs and outputs of the system as desired. For a numerical analysis and study, the system in steady-state is desired, hence the numerical matrices were obtained and linearized around a steady state point. This arbitrary chosen equilibrium

point is where the load is 1166 W (77.7% of the inverter nominal power). For this case, matrices A, B, C and D are shown below:

$$A = \begin{bmatrix}
0 & -3401 & 0 & 0 & 0 & 4.082e5 & 0 & 314 & -0.102 & 0 & 0.5101 & 0 & 0 & 0 \\
3.623e4 & -1.603e4 & 1.603e4 & -3.623e4 & 0 & 0 & 0 & 0 & 314 & 0 & 0 & 0 & 0 & 0 \\
0 & 1.603e4 & -1.603e4 & 0 & 0 & 0 & 0 & 0 & 0.146 & 314 & -0.7322 & 0 & 0 & 0 \\
0 & 3401 & 0 & -1.701e4 & 0 & 0 & 0 & 0 & 0.027 & 0 & 313.9 & 0 & 0 & 0 \\
-470 & -2100 & 0 & -1099 & 0 & 0 & 940 & 0 & 4.057 & 0 & 0 & 0 & 0 & 0 \\
-145.7 & 182.4 & 0 & -340.7 & 310 & -1e5 & 291.4 & -76.94 & 1.283 & 0 & -0.125 & 0 & 0 & 0 \\
0 & -22.34 & 0 & -11.69 & 0 & 0 & 0 & 0 & 0.043 & 0 & 0 & 0 & 0 & 0 \\
-314 & 0.027 & 0 & 0 & 0 & 0 & 0 & 0 & -3400 & 0 & -7.483 & 0 & 4.082e5 & 0 \\
0 & -313.9 & 0 & 0 & 0 & 0 & 0 & 3.623e4 & -1.602e4 & 1.603e4 & -3.627e4 & 0 & 0 & 0 \\
0 & 0.138 & -314 & 0 & 0 & 0 & 0 & 0 & 1.604e4 & -1.603e4 & -37.38 & 0 & 0 & 0 \\
0 & 0.027 & 0 & -314 & 0 & 0 & 0 & 0 & 3403 & 0 & -1.701e4 & 0 & 0 & 0 \\
0 & 0 & 0 & 0 & 0 & 0 & 0 & -470 & -1880 & 0 & 0 & 0 & 0 & 940 \\
76.94 & -0.007 & 0 & 0 & 0 & 0 & 0 & -145.7 & 250.2 & 0 & 1.833 & 310 & -1e5 & 291.4 \\
0 & 0 & 0 & 0 & 0 & 0 & 0 & 0 & -20 & 0 & 0 & 0 & 0 & 0
\end{bmatrix}$$

$$B = \begin{bmatrix}
0 & 0.7614 & 0 \\
0 & 0 & 0 \\
0 & -1.093 & 0 \\
0 & -0.206 & -37960 \\
1880 & 0 & 0 \\
582.8 & 0.187 & 0 \\
20 & 0 & 0 \\
0 & -11.17 & 0 \\
0 & -55.83 & 0 \\
0 & -55.8 & 0 \\
0 & -11.16 & 701 \\
0 & 0 & 0 \\
0 & 2.737 & 0 \\
0 & 0 & 0
\end{bmatrix}$$

$$C = \begin{bmatrix}
0 & 0 & 0 & 1 & 0 & 0 & 0 & 0 & 0 & 0 & 0 & 0 & 0 & 0 \\
0 & 0 & 0 & 0 & 0 & 0 & 0 & 0 & 0 & 0 & 1 & 0 & 0 & 0 \\
0 & 1 & 0 & 0 & 0 & 0 & 0 & 0 & 0 & 0 & 0 & 0 & 0 & 0 \\
0 & 0 & 0 & 0 & 0 & 0 & 0 & 0 & 1 & 0 & 0 & 0 & 0 & 0
\end{bmatrix}$$

$$D = \begin{bmatrix}
0 & 0 & 0 \\
0 & 0 & 0 \\
0 & 0 & 0 \\
0 & 0 & 0
\end{bmatrix}$$

To analyze the closed loop system stability, considering small disturbances, that is, around the equilibrium point, the eigenvalue analysis method was adopted. Objectively, the eigenvalues λ_i of matrix A shed light on the stability of the system, and are shown below:

$$\lambda_i = 1e4 \begin{bmatrix} -9.8999 + 0.0310i \\ -9.8999 - 0.0310i \\ -2.5808 + 0.0314i \\ -2.5808 - 0.0314i \\ -1.7909 + 0.0302i \\ -1.7909 - 0.0302i \\ -0.2612 + 0.7427i \\ -0.2612 - 0.7427i \\ -0.2653 + 0.6497i \\ -0.2653 - 0.6497i \\ -0.1073 + 0.0000i \\ -0.1086 + 0.0000i \\ -0.0010 + 0.0000i \\ -0.0010 + 0.0000i \end{bmatrix}$$

Clearly, it is possible to verify that all eigenvalues have a negative real part, indicating that the system is stable around the equilibrium point. In addition, it is possible to verify 5 pairs of complex poles conjugated, with oscillation frequencies from close to the nominal frequency to high frequencies. The lowest oscillation frequency that appears is 49.338 Hz, while the highest reaches 1.18 kHz. As the average model was considered, the high frequencies that would be related to the switching frequency (hundreds of kHz) do not appear in the model. The dynamics that dominate in the inverter's behavior, are mainly imposed by the poles closest to the origin. Therefore, the real poles have in this case have the strongest impact on dynamics. In addition, as shown in the nonlinear simulations, the system is characterized as stable for a wide range of disturbances (with the projected gains). To see the behavior of the linear system, a step was applied at the input that concerns Z_{load}, which indirectly dictates how much power the load demands. This is a way used to simulate the closed-loop system (as already modeled) for comparison. The model built for this simulation is found in Figure 25, where it is possible to see the system with 3 inputs and 4 outputs.

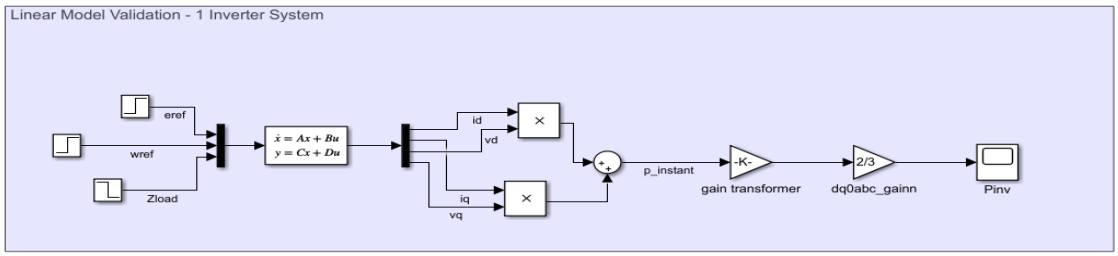

Figure 25 Model developed for validation of the linear model

For quick comparison, the applied step was calculated in order to represent the operating point used for the construction of the matrices (P_{load}= 1166 W) for the nominal power of the inverter (P_{load} = 1500W). In this way, it is possible to check the output power response calculated through the instantaneous power in dq0, and then transformed to abc.

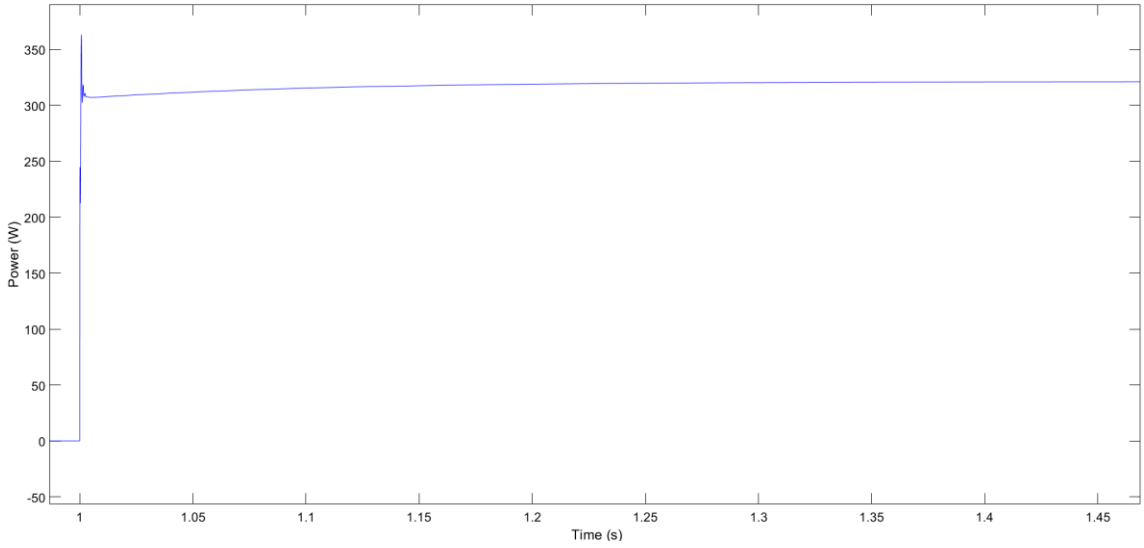

Figure 26 Output Power

Objectively, we can see a step of around 334 W, as expected in the response of the inverter. This validates the obtained linear model.

4.2 Results for the Parallel Inverters Operation Feeding a Isolated Load

This section aims to present the results obtained for the simulations of the parallel operation of two inverters feeding an isolated load. It is important to note that the inverters are identical, that is, they have the same nominal power, the same parameters for the designed LCL filter, as well as the current and voltage controllers. Figure 27 and Figure 28 show the Simulink models developed for the parallel inverters and the droop controls for the inverters, respectively.

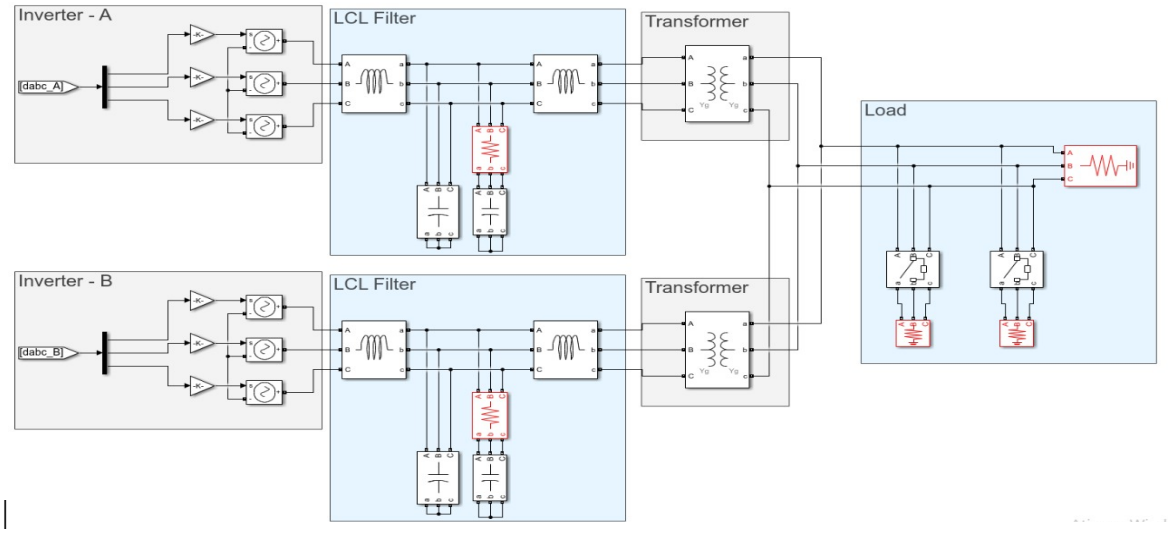

Figure 27 Parallel inverters feeding a isolated load

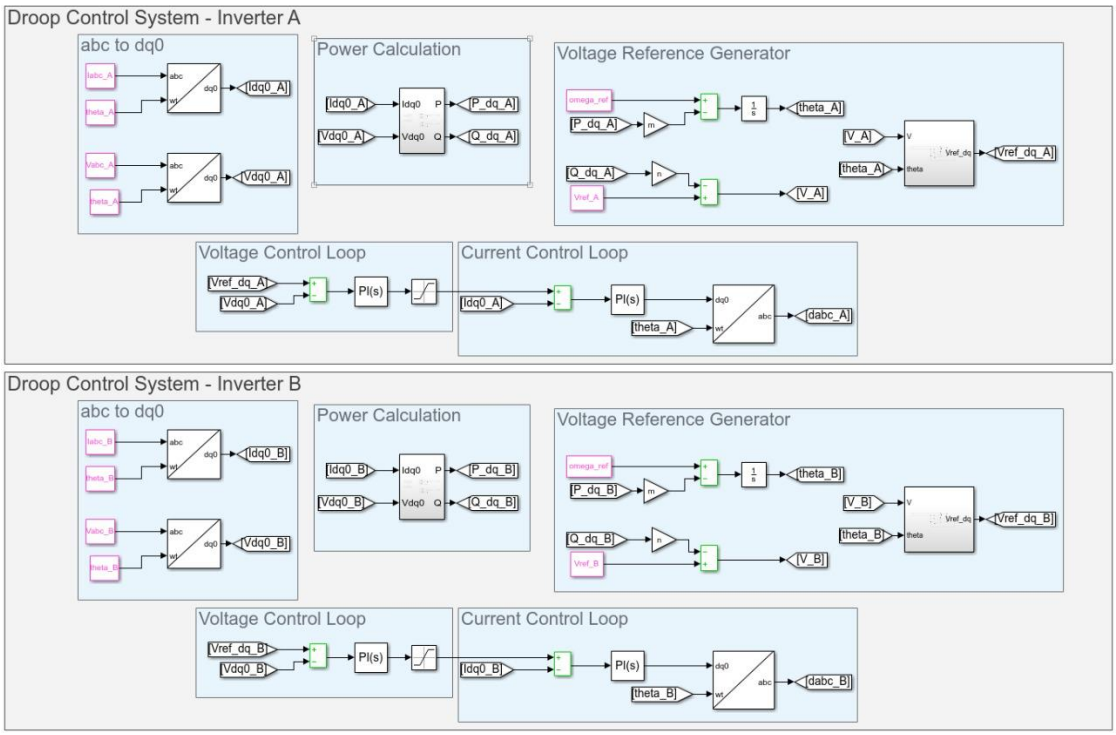

Figure 28 Individual inverters control

Due to this operating condition, the two inverters are considered grid forming, since they have identical characteristics and tend to dictate the behavior of the output voltage and frequency, which will be supplied to the load. The two inverters are connected to the same input DC bus

and to the same output AC bus. As the inverters are equipped with the droop control, they are expected to share power when the load varies, the inverters must maintain the balance of generation and load, each of which must inject a portion of the power demanded by the load. Also, as they have the same characteristics for controllers (same control design), the two must share the output power equally.

In this Chapter, the two inverters will be shown in results as “inv-A” and “inv-B”. Like the previous sections, the results in this section were found for three scenarios, described below:

- **Scenario 1:** The system starts with a load of 2 kW, and at 1 second, a load of 1 kW is switched, reaching the nominal power of the inverter, and at t = 2s, the load of 1 kW is removed, returning to operation with 2 kW.
- **Scenario 2**: The system starts with a load of 200 W, and at 1 second, a load of 3 kW is switched, reaching the nominal power of the inverter, and at t = 2s, the load of 500 W is removed, returning to operation with 200 W.
- **Scenario 3**: Scenario 3 is the again most critical scenario. As in the previous case, to test the limits imposed on the control, an overload of the load is imposed. The system starts with a load of 2 kW, and at t = 1s, a 1 kW load is switched, reaching the nominal power of the inverters (3 kW), and at t = 2s, a load of 2 kW is added, for a total load of 5 kW (166% of the nominal power of the inverters).

4.2.1 Scenario 1

Starting with the least critical scenario, where the load step is not close to the maximum load variation supported by the inverters, Figure 29 and Figure 30 show the powers of the two inverters and the power delivered to the load, and the load current, respectively.

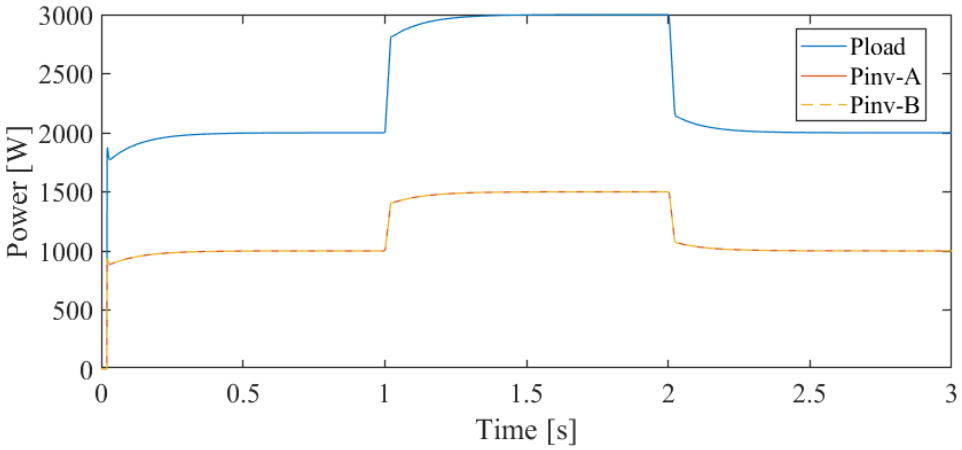

Figure 29 Output Power and Load Power

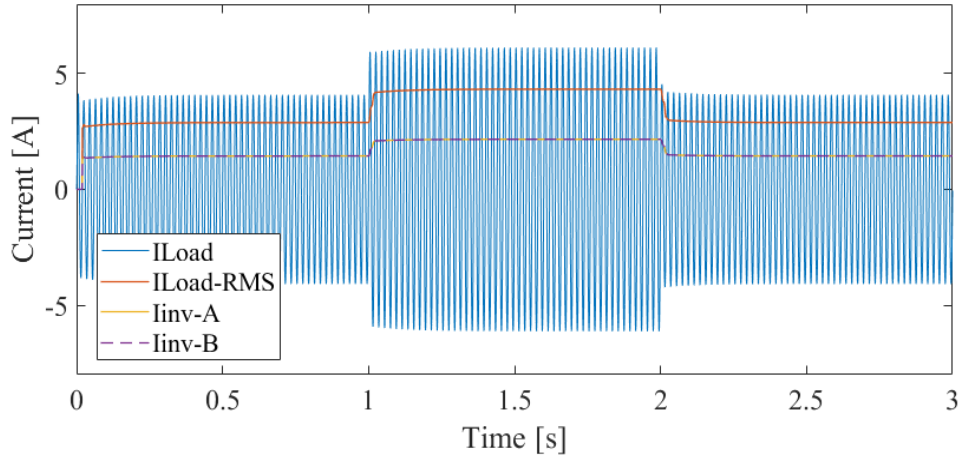

Figure 30 Load Current (Line and RMS)

From Figure 29 and Figure 30, it is possible to determine the sharing of power from the droop control. To meet the load demand, which is switched to 3 kW, the two inverters operate at rated power between 1 s and 2 s, maintaining frequency and voltage within the specified limits, as can be seen in Figure 31 and Figure 32.

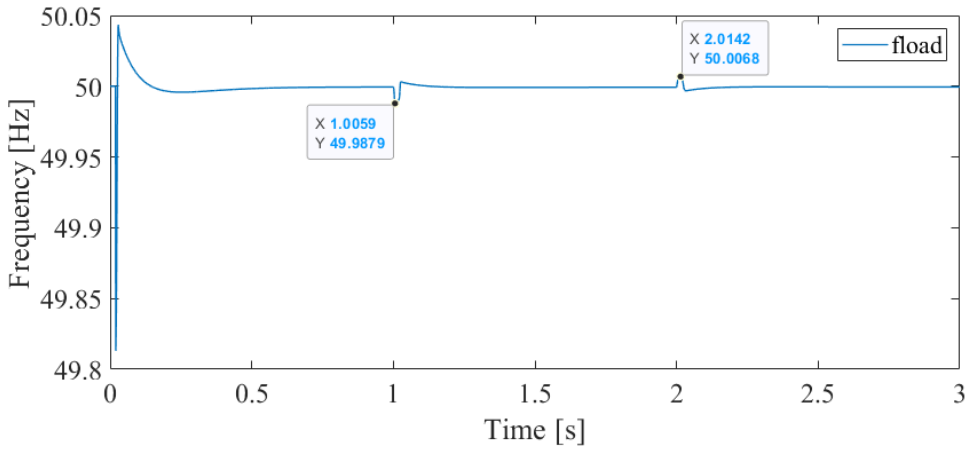

Figure 31 Load Frequency

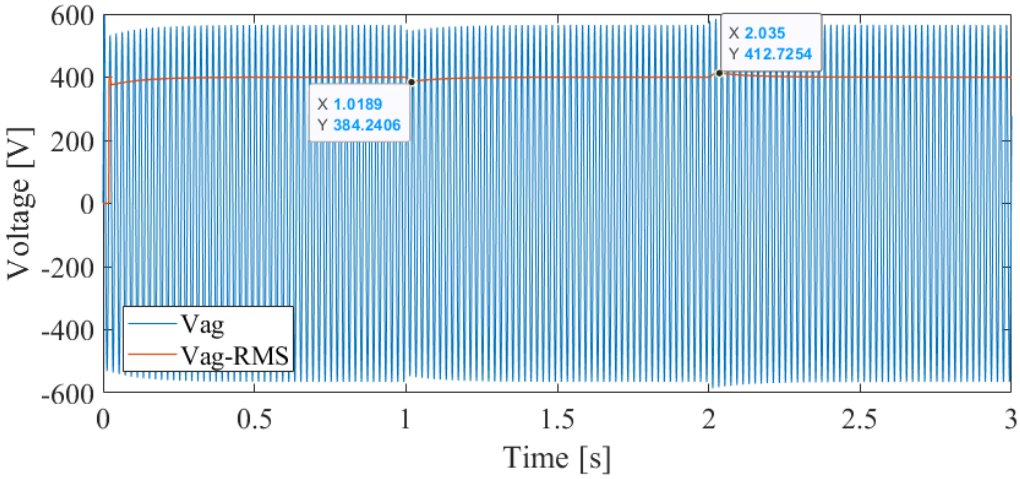

Figure 32 Load Voltage (Line and RMS)

4.2.2 Scenario 2

Scenario 2 presents the scenario where the imposed load step reaches almost 100% of the nominal power of the two inverters. It is in this scenario that the performance of the droop control is shown, mainly evaluating the voltage and frequency drops. For this approach, Figure 33 and Figure 34 show the powers, and the current injected into the load.

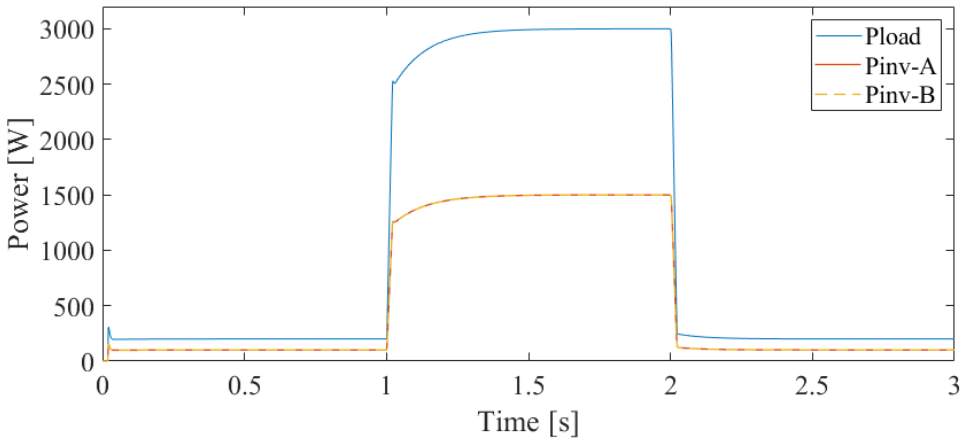

Figure 33 Output Power and Load Power

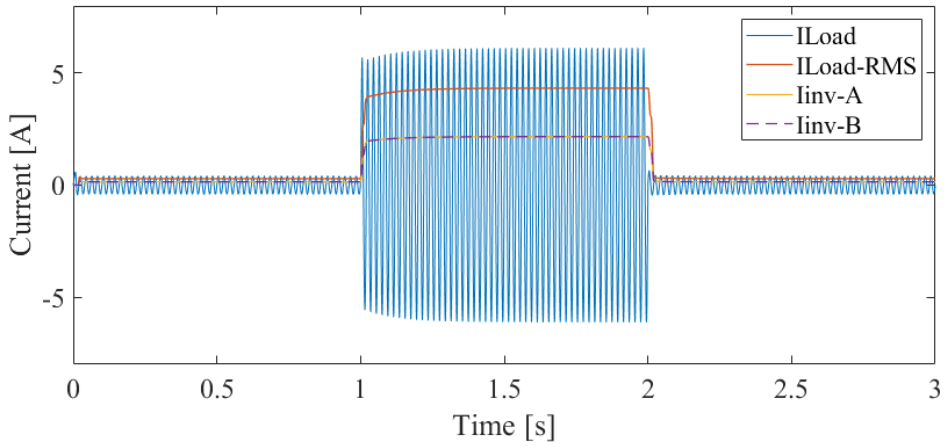

Figure 34 Load Current (Line and RMS)

Clearly, the power sharing takes place between the inverters when supplying the load, being in exactly the same proportion, since the inverters are identical and the droop controls have the same gains. In order to evaluate it even better, Figure 35 and Figure 36 present the frequency and voltage for these load switches.

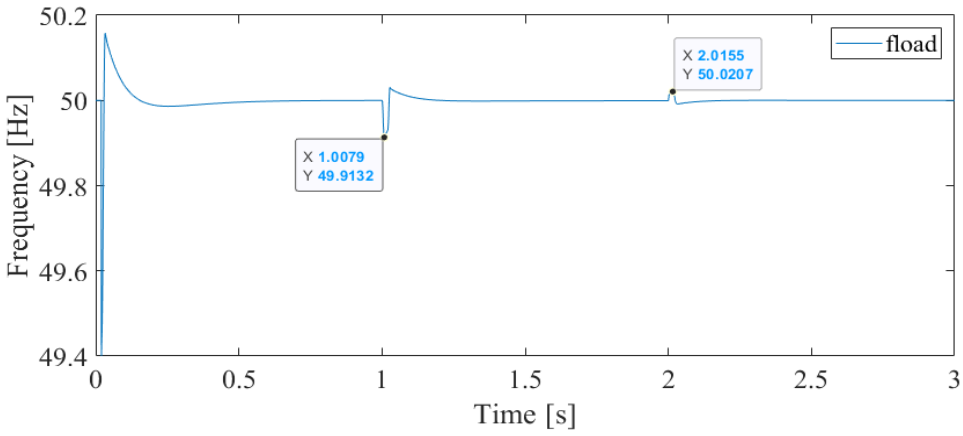

Figure 35 Load Frequency

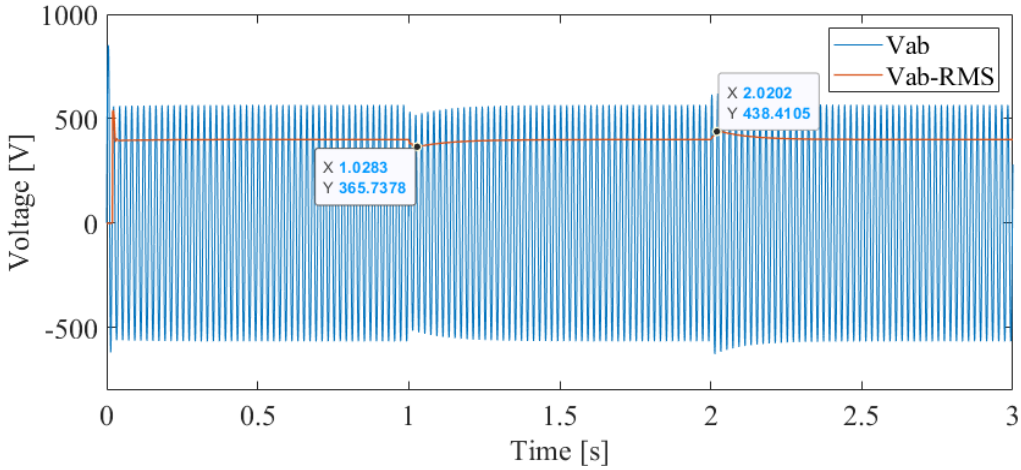

Figure 36 Load Voltage (Line and RMS)

In this case, there is a drop in frequency to 49.91 Hz, which represents a 0.17% drop in relation to the nominal frequency. Regarding the voltage, when the load is switched at t = 1s, the voltage in the load drops to 365.74 V, which represents a 9.37% deviation from the nominal voltage. Even so, both, frequency and voltage, match the control specifications of the droop mesh, presenting a satisfactory performance.

4.2.3 Scenario 3

To evaluate the saturators implemented in the controls loop, an overload is imposed on the inverters. Figure 37, Figure 38, Figure 39 and Figure 40 show respectively, the powers, load currents, frequency and voltage.

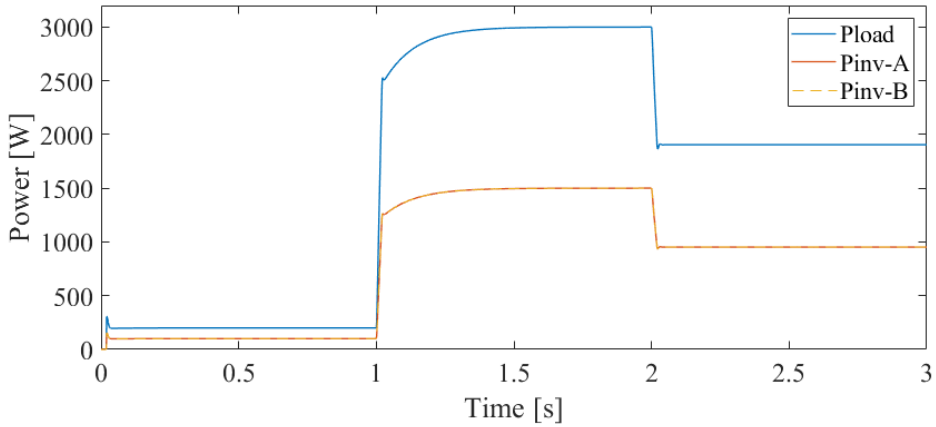

Figure 37 Output Power and Load Power

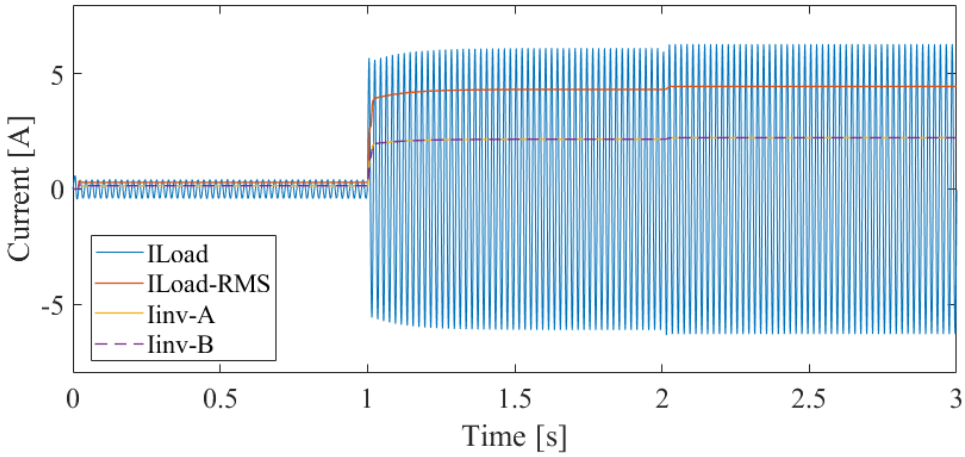

Figure 38 Load Current (Line and RMS)

Like Scenario 3 in the case of an inverter only, the inverters limit the output current, consequently limiting their respective output powers, at t=2s.

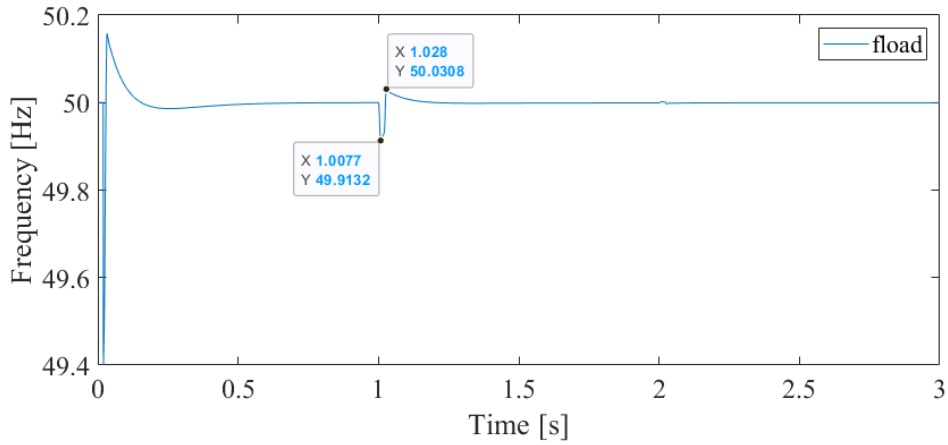

Figure 39 Load Frequency

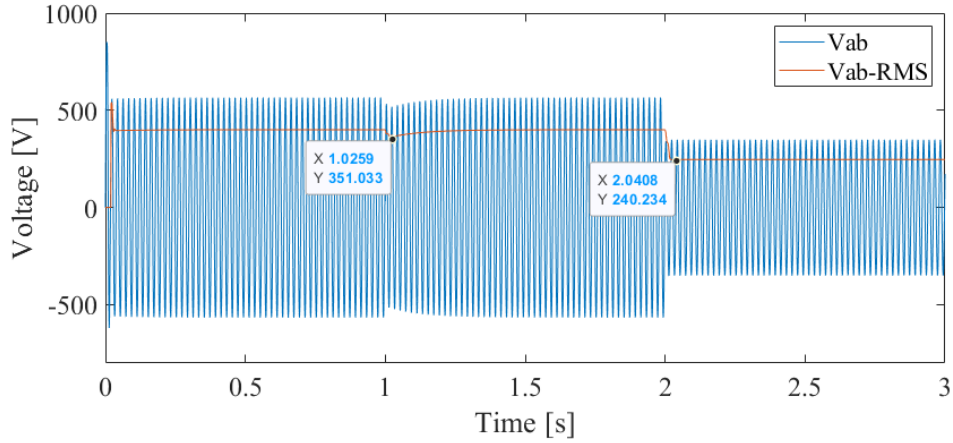

Figure 40 Load Voltage (Line and RMS)

In the same way, the output voltage drops, which is a consequence of the overload, for there to be a balance. The frequency deviation at t = 2s is minimal, since just as the output power of the inverters drops, the load power is also cut, so the difference between generation and load is minimal.

4.2.4 State Space Model

In this section, the parallel operation of the inverters is taken to the state space model. The system modeling for this follows [45]. Assuming that the inverters are connected to the same DC bus and AC bus (and in fact they are), and as the inverters have the same characteristics,

same projected gains and parameters, modeling is facilitated, since the same equations are maintained. The author points out that the reduced-order model, as it is called, maintains the same order, and features of the model for a single inverter, distinguishing by parameters that multiply or divide N, which is the number of inverters in parallel. The impedance of the LCL filter for example is $1/N$ of the impedance of the individual inverter. The gains of the voltage controllers are multiplied by N, and the current gains are divided by N.

Likewise, as state variables are modified according to the number of inverters in the setup. Then, it is possible to develop a generic algorithm for state space modeling, with the variable N as an input parameter, and the model will change little compared to the case of a single inverter. In this way, following [45], analogously to the system of a single inverter only, the generic matrices are presented in the Appendix for this case. Again, the generic system developed for inverters operating in parallel, equipped with the droop control, is seen as a significant contribution of the work, since as mentioned before, generally, the generic models are developed only for the inverter + filter set.

Considering now an arbitrary operating point, where the load is 2691.4 W (89.7%) of the inverter nominal power), the numerical matrices are obtained for this case, shown below:

$$A = 1e5 \begin{bmatrix} 0 & -0.0340 & 0 & 0 & 0 & 4.0816 & 0 & 0.0016 & 0 & 0 & 0 & 0 & 0 & 0 \\ 0.3623 & -0.3206 & 0.3206 & -0.3623 & 0 & 0 & 0 & 0 & 0.0063 & 0 & 0 & 0 & 0 & 0 \\ 0 & 0.3206 & -0.3206 & 0 & 0 & 0 & 0 & 0 & 0 & 0.0063 & 0 & 0 & 0 & 0 \\ 0 & 0.0340 & 0 & -0.1701 & 0 & 0 & 0 & 0 & 0 & 0 & 0.0016 & 0 & 0 & 0 \\ -0.0024 & -0.0420 & 0 & -0.0022 & 0 & 0 & 0.0094 & 0 & 0 & 0 & 0 & 0 & 0 & 0 \\ -0.0024 & 0.0018 & 0 & -0.0034 & 0.0015 & -1 & 0.0015 & -0.0004 & 0 & 0 & 0 & 0 & 0 & 0 \\ 0 & -0.0004 & 0 & 0.0002 & 0 & 0 & 0 & 0 & 0 & 0 & 0 & 0 & 0 & 0 \\ -0.0016 & 0 & 0 & 0 & 0 & 0 & 0 & 0 & -0.034 & 0 & 0 & 0 & 4.0816 & 0 \\ 0 & -0.0063 & 0 & 0 & 0 & 0 & 0 & 0.3623 & -0.3205 & 0.3206 & -0.3631 & 0 & 0 & 0 \\ 0 & 0 & -0.0063 & 0 & 0 & 0 & 0 & 0 & 0.3208 & -0.3206 & -0.0007 & 0 & 0 & 0 \\ 0 & 0 & 0 & -0.00016 & 0 & 0 & 0 & 0 & 0.0340 & 0 & -0.1701 & 0 & 0 & 0 \\ 0 & 0 & 0 & 0 & 0 & 0 & 0 & -0.0024 & -0.0376 & 0 & 0 & 0 & 0 & 0.0094 \\ 0.0004 & 0 & 0 & 0 & 0 & 0 & 0 & -0.0004 & 0.0025 & 0 & 0 & 0.0015 & -1 & .0015 \\ 0 & 0 & 0 & 0 & 0 & 0 & 0 & 0 & -0.0004 & 0 & 0 & 0 & 0 & 0 \end{bmatrix}$$

$$B = 1e4\begin{bmatrix} 0 & 0.9161 & 0 \\ 0 & 0 & 0 \\ 0 & -2.1865 & 0 \\ 0 & -0.0515 & -37972 \\ 3760 & 0 & 0 \\ 582.8 & -0.2244 & 0 \\ 40 & 0 & 0 \\ 0 & -5.5914 & 0 \\ 0 & -111.65 & 0 \\ 0 & -111.6 & 0 \\ 0 & -5.5819 & 350.64 \\ 0 & 0 & 0 \\ 0 & 1.3699 & 0 \\ 0 & 0 & 0 \end{bmatrix}$$

$$C = \begin{bmatrix} 0 & 0 & 0 & 1 & 0 & 0 & 0 & 0 & 0 & 0 & 0 & 0 & 0 & 0 \\ 0 & 0 & 0 & 0 & 0 & 0 & 0 & 0 & 0 & 0 & 1 & 0 & 0 & 0 \\ 0 & 1 & 0 & 0 & 0 & 0 & 0 & 0 & 0 & 0 & 0 & 0 & 0 & 0 \\ 0 & 0 & 0 & 0 & 0 & 0 & 0 & 0 & 1 & 0 & 0 & 0 & 0 & 0 \end{bmatrix}$$

$$D = \begin{bmatrix} 0 & 0 & 0 \\ 0 & 0 & 0 \\ 0 & 0 & 0 \\ 0 & 0 & 0 \end{bmatrix}$$

Analyzing the closed-loop stability of the system, the poles of the closed-loop system, given by the eigenvalues of the linearized state matrix A, are shown below:

$$\lambda_i = 1e4\begin{bmatrix} -9.9228 + 0.0129i \\ -9.9228 - 0.0129i \\ -6.2583 + 0.0653i \\ -6.2583 - 0.0653i \\ -0.1856 + 0.7671i \\ -0.1856 - 0.7671i \\ -0.1887 + 0.6611i \\ -0.1887 - 0.6611i \\ -1.4691 + 0.0000i \\ -1.4273 + 0.0000i \\ -0.1082 + 0.0014i \\ -0.1082 - 0.0014i \\ -0.0010 + 0.0000i \\ -0.0010 - 0.0000i \end{bmatrix}$$

Again, for the system with two inverters operating in parallel, supplying an isolated load, the closed-loop system is stable around the considered equilibrium point. It is possible to verify 6 pairs of conjugated complex poles, with frequencies from 0.00022 Hz (lowest) to 1.22 kHz (highest).

Like the first case, the real pole appears as the dominant pole, as it is closer to the origin. The analysis could extend to other equilibrium points, respecting the power limits of the inverters. However, the analysis of the non-linear results presented in the previous sections allows us to conclude that the system has a stable closed-loop behavior for the entire region. Where the load demands less power than the sum of the rated powers of the inverters. Also, if the limiters are

acting as load shedding in the inverters controls, the system can maintain stability even for disturbances greater than its capacity, obviously, with the load partially fed. For the validation of the obtained linear model, a load step (through the variable Z_{load}) was applied and the output power of the linear model was calculated, in the same way that it was done for the case of the individual inverter. As previously adopted, the equilibrium point for obtaining the numerical matrices was for a load of 2691.4W, so the step applied starts from this point to the sum of the nominal capacities of the inverters (3 kW). Figure 42 shows the load power calculated using the linearized model. The model used to validate the linear model is the same for the case of 1 inverter only, differentiating only in the declared matrices, and it is shown in Figure 41.

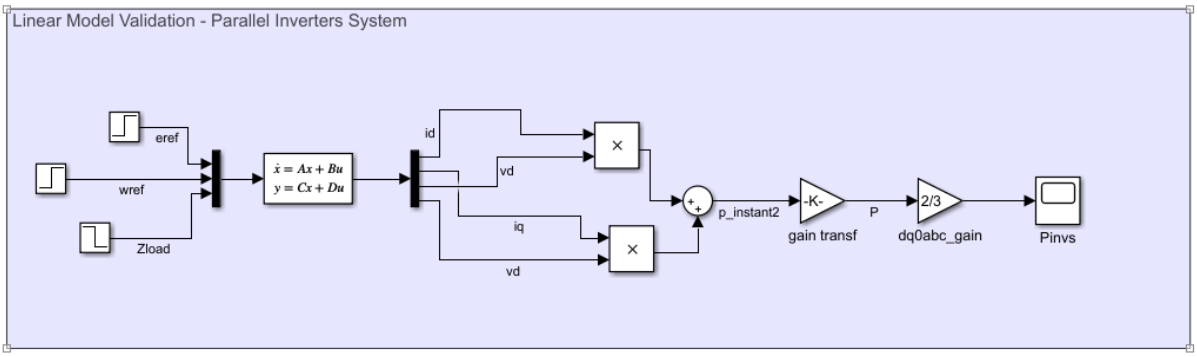

Figure 41 Model developed for validation of the parallel system linear model

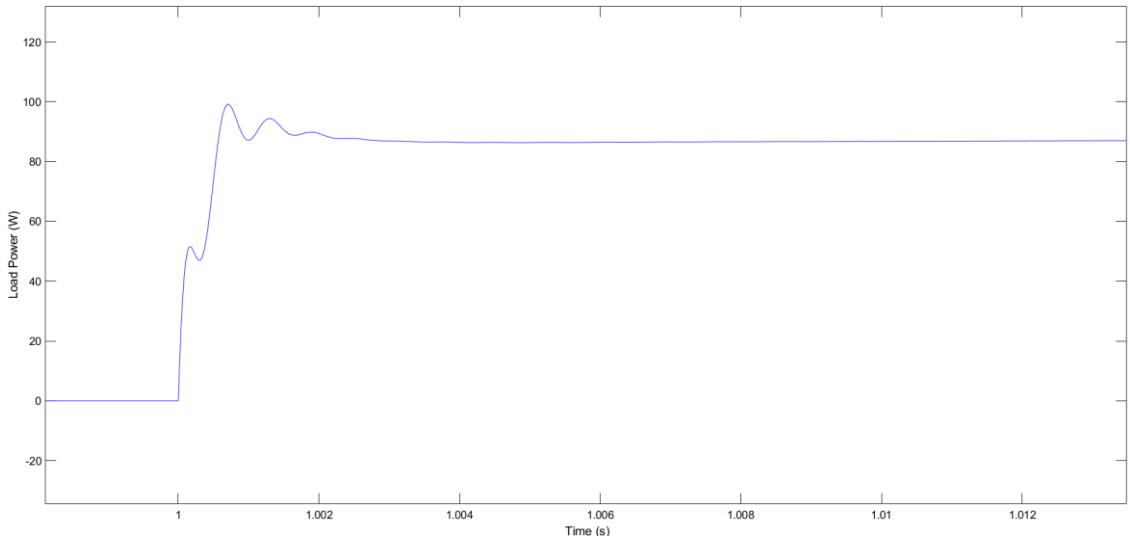

Figure 42 Output Power

From Figure 42, it is possible to notice the step of approximately 85W at the output, feeding the load. This value was expected, due to the associated modeling. In this way, the mathematical model developed is validated, and can be used in numerous approaches.

5 CONCLUSIONS

The growth of intermittent sources in the global energy matrix is irreversible, and together with this, challenges arise with regard to the control, efficiency and protection of power systems. Distributed generation affects already consolidated systems in several areas. Despite considerable research in this area in recent years, there are still challenges to be addressed. In that context, this work sought to develop droop control in the isolated operation of inverters feeding the load. The conventional droop strategy does not need lines of communication between the inverters in parallel operation, which is the main advantage of this application. As it is a not very complex strategy, it also has its limitations.

It was possible to observe the advantages of the droop control from the obtained results. The restoration of voltage and frequency in the load in the event of a disturbance is achieved quickly, controlling the injection / absorption of power by the inverter. Also, in parallel operation of the inverters, the power sharing between them is effectively achieved, operating together to maintain the voltage and frequency limits on the load.

Furthermore, the work approached the state space modeling of the system. Generally, in the literature, what is most seen is the mathematical modeling of the inverter + filter, however, this work brought the implementation of an algorithm capable of providing the complete and generic modeling of the system as a whole, including voltage and current controls, beyond droop control, that is, considering all control loops involved in the system. This is understood as a significant contribution of the work to the area.

5.1 Future Work

This work opens up the possibility of future studies, which were not emphasized in this work. Some ideas for future work are:

- Evaluate the performance of the implemented system against the microgrid connection.
- Expand the analysis to inverters with different characteristics, that is, with fixed parameters, control parameters and different nominal powers.
- Make a comparison between droop control strategies present in the literature.
- Extend the analysis by considering the intermittency of the primary energy source.

WORK CITED

[1] N. Hatziargyriou, H. Asano, R. Iravani, and C. Marnay, "Microgrids," *IEEE Power Energy,* vol. 6, no. 3, pp. 26-29, 2008.

[2] H. M. Kojabadi, B. Yu, I. A. Gadoura, L. Chang, and M. Ghribi, "A novel DSP-based current-controlled PWM strategy for single phase grid connected inverters," *IEEE transactions on power electronics,* vol. 21, no. 4, pp. 985-993, 2006.

[3] J. C. Moreno, J. M. E. Huerta, R. G. Gil, and S. A. Gonzalez, "A robust predictive current control for three-phase grid-connected inverters," *IEEE Transactions on Industrial Electronics,* vol. 56, no. 6, pp. 1993-2004, 2009.

[4] J. Dannehl, F. W. Fuchs, and P. B. Thøgersen, "PI state space current control of grid-connected PWM converters with LCL filters," *IEEE Transactions on Power Electronics,* vol. 25, no. 9, pp. 2320-2330, 2010.

[5] T.-V. Tran, T.-W. Chun, H.-H. Lee, H.-G. Kim, and E.-C. Nho, "Control for grid-connected and stand-alone operations of three-phase grid-connected inverter," in *2012 International Conference on Renewable Energy Research and Applications (ICRERA)*, 2012: IEEE, pp. 1-5.

[6] Y. Zhang, F. Zhang, Y. Quan, and P. Zhang, "Analysis of Three-Phase Inverter Parallel Operation with Network-Based Control Having Strong Robustness and Wide Time-Scale Compatibility in Droop-Controlled AC Microgrid," *Electronics,* vol. 9, no. 2, p. 376, 2020.

[7] R. S. Kushwah and G. Walke, "Parallel Operation of Inverters With Droop Control of Voltage and Frequency," in *2018 International Conference on Smart City and Emerging Technology (ICSCET)*, 2018: IEEE, pp. 1-5.

[8] A. Elnady and M. AlShabi, "Operation of parallel inverters in microgrid using new adaptive PI controllers based on least mean fourth technique," *Mathematical Problems in Engineering,* vol. 2019, 2019.

[9] K. T. Tan, X. Peng, P. L. So, Y. C. Chu, and M. Z. Chen, "Centralized control for parallel operation of distributed generation inverters in microgrids," *IEEE Transactions on Smart Grid*, vol. 3, no. 4, pp. 1977-1987, 2012.

[10] A. Mohd, E. Ortjohann, D. Morton, and O. Omari, "Review of control techniques for inverters parallel operation," *Electric Power Systems Research,* vol. 80, no. 12, pp. 1477-1487, 2010.

[11] S. Wang, Z. Liu, J. Liu, R. An, and M. Xin, "Breaking the boundary: A droop and master-slave hybrid control strategy for parallel inverters in islanded microgrids," in *2017 IEEE Energy Conversion Congress and Exposition (ECCE)*, 2017: IEEE, pp. 3345-3352.

[12] P. Ye *et al.*, "An improved droop control strategy for parallel inverters in microgrid," in *2017 IEEE Conference on Energy Internet and Energy System Integration (EI2)*, 2017: IEEE, pp. 1-5.

[13] E. Rokrok and M. E. H. Golshan, "Adaptive voltage droop scheme for voltage source converters in an islanded multibus microgrid," *IET generation, transmission & distribution,* vol. 4, no. 5, pp. 562-578, 2010.

[14] T. Chen, O. Abdel-Rahim, F. Peng, and H. Wang, "An Improved Finite Control Set-MPC-Based Power Sharing Control Strategy for Islanded AC Microgrids," *IEEE Access,* vol. 8, pp. 52676-52686, 2020.

[15] U. B. Tayab, M. A. B. Roslan, L. J. Hwai, and M. Kashif, "A review of droop control techniques for microgrid," *Renewable and Sustainable Energy Reviews,* vol. 76, pp. 717-727, 2017.

[16] K. Wang, X. Huang, B. Fan, Q. Yang, G. Li, and M. L. Crow, "Decentralized power sharing control for parallel-connected inverters in islanded single-phase micro-grids," *IEEE Transactions on Smart Grid,* vol. 9, no. 6, pp. 6721-6730, 2017.

[17] S. Bera, D. K. Mandal, and S. Chowdhuri, "Improved Droop Control Strategy for Single Phase Micro-Grid Inverters in Stand-Alone Mode," in *2019 International Conference on Computing, Power and Communication Technologies (GUCON)*, 2019: IEEE, pp. 811-816.

[18] E. Alizadeh, A. M. Birjandi, and M. Hamzeh, "Decentralised power sharing control strategy in LV microgrids under unbalanced load conditions," *IET Generation, Transmission & Distribution,* vol. 11, no. 7, pp. 1613-1623, 2017.

[19] H. Han, X. Hou, J. Yang, J. Wu, M. Su, and J. M. Guerrero, "Review of power sharing control strategies for islanding operation of AC microgrids," *IEEE Transactions on Smart Grid,* vol. 7, no. 1, pp. 200-215, 2015.

[20] L. Lei, M. A. Elgendy, N. Wade, and S. Ethni, "Power sharing between parallel inverters by using droop control with a secondary control loop," in *2019 IEEE 10th International Symposium on Power Electronics for Distributed Generation Systems (PEDG)*, 2019: IEEE, pp. 653-658.

[21] H. Moussa, A. Shahin, J.-P. Martin, B. Nahid-Mobarakeh, S. Pierfederici, and N. Moubayed, "Harmonic power sharing with voltage distortion compensation of droop controlled islanded microgrids," *IEEE Transactions on Smart Grid*, vol. 9, no. 5, pp. 5335-5347, 2017.

[22] A. Khorsandi, M. Ashourloo, H. Mokhtari, and R. Iravani, "Automatic droop control for a low voltage DC microgrid," *IET Generation, Transmission & Distribution*, vol. 10, no. 1, pp. 41-47, 2016.

[23] J. Yu, W. Ming, L. Haitao, L. Yang, and Z. Ying, "Bidirectional droop control of interlinking converter in ac/dc hybrid micro-grid," in *2016 3rd International Conference on Information Science and Control Engineering (ICISCE)*, 2016: IEEE, pp. 879-883.

[24] S. I. Gkavanoudis, K. O. Oureilidis, and C. S. Demoulias, "An adaptive droop control method for balancing the SoC of distributed batteries in AC microgrids," in *2016 IEEE 17th Workshop on Control and Modeling for Power Electronics (COMPEL)*, 2016: IEEE, pp. 1-6.

[25] Y. Xia, Y. Peng, P. Yang, M. Yu, and W. Wei, "Distributed coordination control for multiple bidirectional power converters in a hybrid AC/DC microgrid," *IEEE Transactions on Power Electronics*, vol. 32, no. 6, pp. 4949-4959, 2016.

[26] H. Xiao, A. Luo, Z. Shuai, G. Jin, and Y. Huang, "An improved control method for multiple bidirectional power converters in hybrid AC/DC microgrid," *IEEE Transactions on Smart Grid*, vol. 7, no. 1, pp. 340-347, 2015.

[27] N. Hajilu, G. Gharehpetian, S. Hosseinian, M. Poursistani, and M. Kohansal, "Power control strategy in islanded microgrids based on VF and PQ theory using droop control of inverters," in *2015 International Congress on Electric Industry Automation (ICEIA 2015)*, 2015: IEEE, pp. 37-42.

[28] S. Mansour, M. I. Marei, and A. A. Sattar, "Decentralized secondary control for frequency restoration of microgrids with VF and PQ droop controlled inverters," in *2017 Nineteenth International Middle East Power Systems Conference (MEPCON)*, 2017: IEEE, pp. 1170-1176.

[29] X. Meng, J. Liu, and Z. Liu, "A generalized droop control for grid-supporting inverter based on comparison between traditional droop control and virtual synchronous generator control," *IEEE Transactions on Power Electronics*, vol. 34, no. 6, pp. 5416-5438, 2018.

[30] P. Monica, M. Kowsalya, and K. Subramanian, "Droop Reference based decoupling coupling control of NPC inverter for islanded microgrid," in *2017 Innovations in Power and Advanced Computing Technologies (i-PACT)*, 2017: IEEE, pp. 1-5.

[31] W. Cao, H. Su, J. Cao, J. Sun, and D. Yang, "Improved droop control method in microgrid and its small signal stability analysis," in *2014 International Conference on Renewable Energy Research and Application (ICRERA)*, 2014: IEEE, pp. 197-202.

[32] K. Yu, Q. Ai, S. Wang, J. Ni, and T. Lv, "Analysis and optimization of droop controller for microgrid system based on small-signal dynamic model," *IEEE Transactions on Smart Grid*, vol. 7, no. 2, pp. 695-705, 2015.

[33] E. Barklund, N. Pogaku, M. Prodanovic, C. Hernandez-Aramburo, and T. C. Green, "Energy management in autonomous microgrid using stability-constrained droop control of inverters," *IEEE Transactions on Power Electronics*, vol. 23, no. 5, pp. 2346-2352, 2008.

[34] S. Eberlein and K. Rudion, "Small-signal stability modelling, sensitivity analysis and optimization of droop controlled inverters in LV microgrids," *International Journal of Electrical Power & Energy Systems*, vol. 125, p. 106404, 2021.

[35] A. U. Krismanto, N. Mithulananthan, and A. Lomi, "Dynamic droop control in microgrid for stability enhancement considering RES variation," in *2017 IEEE PES Innovative Smart Grid Technologies Conference Europe (ISGT-Europe)*, 2017: IEEE, pp. 1-6.

[36] T. Remus, L. Marco, and R. Pedro, "Grid Converter Control for WTS," in *Grid Converters for Photovoltaic and Wind Power Systems*: IEEE, 2007, pp. 205-236.

[37] M. Liserre, F. Blaabjerg, and S. Hansen, "Design and control of an LCL-filter-based three-phase active rectifier," *I E E E Transactions on Industry Applications*, Journal article vol. 41, no. 5, pp. 1281-1291, 2005.

[38] M. Liserre, F. Blaabjerg, and A. D. Aquila, "Step-by-Step Design Procedure for a Grid-Connected Three-Phase PWM Voltage Source Converter," *International Journal of Electronics*, Journal article vol. 91, no. 8, pp. 445-460, 2004.

[39] S. Hiti, "Modeling and control of three-phase PWM converters," Virginia Tech, 1995.

[40] P. Xuetao, Y. Tiankai, Q. Keqing, Z. Jinbin, L. Wenqi, and C. Xuhui, "Analysis and evaluation of the decoupling control strategies for the design of grid-connected inverter with LCL filter," in *International Conference on Renewable Power Generation (RPG 2015)*, 17-18 Oct. 2015 2015, pp. 1-6, doi: 10.1049/cp.2015.0530.

[41] W. Dan, T. Fen, J. C. Vasquez, and J. M. Guerrero, "Control and analysis of droop and reverse droop controllers for distributed generations," in *2014 IEEE 11th International Multi-Conference on Systems, Signals & Devices (SSD14)*, 11-14 Feb. 2014 2014, pp. 1-5, doi: 10.1109/SSD.2014.6808842.

[42] W. Tsai-Fu, C. Yu-Kai, and H. Yong-Heh, "3C strategy for inverters in parallel operation achieving an equal current distribution," *IEEE Transactions on Industrial Electronics*, vol. 47, no. 2, pp. 273-281, 2000, doi: 10.1109/41.836342.

[43] J. Kim, B. Kim, J. Cho, J. Lee, and C. Won, "Multinomial model of droop control method for parallel-connected UPS inverters," in *2017 20th International Conference on Electrical Machines and Systems (ICEMS)*, 11-14 Aug. 2017 2017, pp. 1-6, doi: 10.1109/ICEMS.2017.8056241.

[44] D. C. Raj and D. N. Gaonkar, "Frequency and voltage droop control of parallel inverters in microgrid," in *2016 2nd International Conference on Control, Instrumentation, Energy & Communication (CIEC)*, 28-30 Jan. 2016 2016, pp. 407-411, doi: 10.1109/CIEC.2016.7513771.

[45] V. Purba, B. B. Johnson, and S. V. Dhople, "Reduced-order Aggregate Model for Parallel-connected Grid-tied Three-phase Photovoltaic Inverters," in *2019 IEEE 46th Photovoltaic Specialists Conference (PVSC)*, 16-21 June 2019 2019, pp. 0724-0729, doi: 10.1109/PVSC40753.2019.8980475.

APPENDIX

Table A.1 Droop Control Parameters and Implementation

K_{pi}	0.0031
T_{ii}	0.001
K_i	0.470
T_{iv}	$1e-5$
T_s	2
K_{pv}	0.1
K_v	2
$Z_{loadnom}$ (1 inverter system)	3.88 Ω
$Z_{loadnom}$ (2 inverters system)	1.95 Ω

1. Algorithm developed in MATLAB for construction of the state space - System with 1 Inverter

A. Modeling of an inverter connected to the load with Droop control

```
clc;
clear all;
close all;

syms Lc iLcd diLcd iLcq diLcq Cf vCfd dvCfd vCfq dvCfq Cd vCdd dvCdd vCdq dvCdq Lr iLrd diLrd iLrq diLrq Zload
syms Rd vGd vGq md mq E y1 y2 y3 y4 y RLc RLr
syms w
syms igd digd igq digq ki kpi Tii idRef iqRef m2d dm2d m2q dm2q Ts
syms phi P01 w0 Q01 V0 kp kq P0 Q0
syms vb dvb gv dgv kv Tiv kpv
syms vgd dvgd vgq dvgq kv Tiv kpv vdRef vqRef
syms deltaW Pmax deltaV Qmax eRef wRef P Q mdroop ndroop edroop

% Open Loop Equations
eqns = [Lc*diLcd == w*Lc*iLcq - iLcd*RLc + m2d*vb - vCfd,
        Lr*diLrd == w*Lr*iLrq - iLrd*RLr + vCfd - iLrd*Zload,
        Cf*dvCfd == w*Cf*vCfq + iLcd - iLrd - vCfd/Rd + vCdd/Rd,
        Cd*dvCdd == w*Cd*vCdq + vCfd/Rd - vCdd/Rd,
        Lc*diLcq == -w*Lc*iLcd - iLcq*RLc + m2q*vb - vCfq,
        Lr*diLrq == -w*Lr*iLrd - iLrq*RLr + vCfq - iLrq*Zload,
        Cf*dvCfq == -w*Cf*vCfd + iLcq - iLrq - vCfq/Rd + vCdq/Rd,
        Cd*dvCdq == -w*Cd*vCdd + vCfq/Rd - vCdq/Rd,
        digd == (idRef - iLcd)*ki/Tii,
        digq == (iqRef - iLcq)*ki/Tii
        dm2d == (md - m2d)*(1/Ts),
        dm2q == (mq - m2q)*(1/Ts),
```

```
        dvgd == (vdRef - vCfd)*kv/Tiv,
        dvgq == (vqRef - vCfq)*kv/Tiv];


    %Replaces the variables md mq, iRef, vdRef = E and w
eqns = subs(eqns, [md, mq], [(idRef*ki-iLcd*ki+igd)*kpi + vCfd/vb - w*Lc*iLcq/vb, (iqRef*ki-iLcq*ki+igq)*kpi + vCfq/vb + w*Lc*iLcd/vb]);
eqns = subs(eqns, [idRef iqRef], [(vdRef*kv-vCfd*kv+vgd)*kpv, (vqRef*kv-vCfq*kv+vgq)*kpv]);
eqns = subs(eqns, [vdRef w], [eRef-(deltaW/Pmax)*(vCfd*iLrd+vCfq*iLrq), (wRef-(deltaV/Qmax)*(vCfq*iLrd-vCfd*iLrq))]);


% Definition of input and output vectors
x = [iLcd vCfd vCdd iLrd igd m2d vgd iLcq vCfq vCdq iLrq igq m2q vgq];
dx = [diLcd dvCfd dvCdd diLrd digd dm2d dvgd diLcq dvCfq dvCdq diLrq digq dm2q dvgq];

%inputs
u = [eRef, wRef, Zload];

% Solution of the system of equations as a function of the vector dx
S = solve(eqns,dx);
sol = [S.diLcd S.dvCfd S.dvCdd S.diLrd S.digd S.dm2d S.dvgd S.diLcq S.dvCfq S.dvCdq S.diLrq S.digq S.dm2q S.dvgq];

% Linearization of equations
linSol = jacobian(sol,[x,u]);

Alin = linSol(:,1:length(x))
Blin = linSol(:,length(x)+1:end)

%Output equations
eqns_output = [y1 == iLrd,
               y2 == iLrq,
               y3 == vCfd,
               y4 == vCfq];
% Vector definition
y = [y1, y2, y3, y4];
```

```
S_out = solve(eqns_output,y);
sol_out = [S_out.y1, S_out.y2,S_out.y3,S_out.y4];

linSolOut = jacobian(sol_out,[x,u]);

Clin = linSolOut(:,1:length(x))
Dlin = linSolOut(:,length(x)+1:end)

parameters = [Lc, Cf, Cd, Rd, Lr, vGd, vGq, kpi, Tii, ki, Ts, vdRef, vqRef,vb, RLc, RLr, kpv, Tiv, kv, Zload, deltaW, Pmax, deltaV, Qmax, eRef,
wRef, vqRef]
parameters_value = [294e-6, 27.6e-6, 27.6e-6, 3.26, 294e-6, 62.35, 0, 0.0031, 1/1e3, 0.470, 1e-5,...
                    11, 0, 120, 0.000025, 0.000025, 2, 1/10, 2, 5, 2*3.14159*2.5, 1500, 6, 500, 62.35, 2*3.14159*50, 0];

% Solution in steady state
eqnsSS = subs(eqns,[parameters dx],[parameters_value zeros(1,length(dx))]);
S_SS = solve(eqnsSS,x)
solSS = double([S_SS.iLcd(1) S_SS.vCfd(1) S_SS.vCdd(1) S_SS.iLrd(1) S_SS.igd(1) S_SS.m2d(1) S_SS.vgd(1) S_SS.iLcq(1) S_SS.vCfq(1) S_SS.vCdq(1)
S_SS.iLrq(1) S_SS.igq(1) S_SS.m2q(1) S_SS.vgq(1)]);

% % Input vector
uSS = [eRef, wRef, Zload];
uSS = double(subs(uSS,parameters, parameters_value));

% Output solution in steady state
solSS_output = double(subs(Clin,[parameters dx],[parameters_value zeros(1,length(dx))]))*solSS'+...
               double(subs(Dlin,[parameters dx],[parameters_value zeros(1,length(dx))]))*uSS';

% Linearized Matrix
AlinNum = double(subs(Alin, [parameters x], [parameters_value solSS]));
BlinNum = double(subs(Blin, [parameters x], [parameters_value solSS]));
ClinNum = double(subs(Clin, [parameters x], [parameters_value solSS]));
DlinNum = double(subs(Dlin, [parameters x], [parameters_value solSS]));

% Representation of the small signal model in state space
ssLinSys = ss(AlinNum,BlinNum,ClinNum,DlinNum)
```

```
% Stability analysis - Poles
poles = pole(ssLinSys)
```

2. Algorithm developed in MATLAB for construction of the state space – Parallel Inverters System

B. Modeling of N inverters connected to the load with Droop control

```
clc;
clear all;
close all;

syms Lc iLcd diLcd iLcq diLcq Cf vCfd dvCfd vCfq dvCfq Cd vCdd dvCdd vCdq dvCdq Lr iLrd diLrd iLrq diLrq Zload
syms Rd vGd vGq md mq E y1 y2 y3 y4 y RLc RLr
syms w N
syms igd digd igq digq ki kpi Tii idRef iqRef m2d dm2d m2q dm2q Ts
syms phi P01 w0 Q01 V0 kp kq P0 Q0
syms vb dvb gv dgv kv Tiv kpv
syms vgd dvgd vgq dvgq kv Tiv kpv vdRef vqRef
syms deltaW Pmax deltaV Qmax eRef wRef P Q mdroop ndroop edroop

% Open Loop Equations
eqns = [Lc*diLcd == w*(Lc/N)*iLcq - iLcd*(RLc/N) + m2d*vb - vCfd,
        Lr*diLrd == w*(Lr/N)*iLrq - iLrd*(RLr/N) + vCfd - iLrd*Zload,
        Cf*dvCfd == w*(N*Cf)*vCfq + iLcd - iLrd - vCfd/(Rd/N) + vCdd/(Rd/N),
        Cd*dvCdd == w*(N*Cd)*vCdq + vCfd/(Rd/N) - vCdd/(Rd/N),
        Lc*diLcq == -w*(Lc/N)*iLcd - iLcq*(RLc/N) + m2q*vb - vCfq,
        Lr*diLrq == -w*(Lr/N)*iLrd - iLrq*(RLr/N) + vCfq - iLrq*Zload,
        Cf*dvCfq == -w*(N*Cf)*vCfd + iLcq - iLrq - vCfq/(Rd/N) + vCdq/(Rd/N),
        Cd*dvCdq == -w*(N*Cd)*vCdd + vCfq/(Rd/N) - vCdq/(Rd/N),
```

```
        digd == (idRef - iLcd)*(ki/N)/Tii,
        digq == (iqRef - iLcq)*(ki/N)/Tii
        dm2d == (md - m2d)*(1/Ts),
        dm2q == (mq - m2q)*(1/Ts),
        dvgd == (vdRef - vCfd)*(N*kv)/Tiv,
        dvgq == (vqRef - vCfq)*(N*kv)/Tiv];


eqns = subs(eqns, [md, mq], [(idRef*(ki/N)-iLcd*(ki/N)+igd)*(kpi/N) + vCfd/vb - w*(Lc/N)*iLcq/vb, (iqRef*(ki/N)-iLcq*(ki/N)+igq)*(kpi/N) +
vCfq/vb + w*(Lc/N)*iLcd/vb]);
eqns = subs(eqns, [idRef iqRef], [(vdRef*(N*kv)-vCfd*(N*kv)+vgd)*(N*kpv), (vqRef*(N*kv)-vCfq*(N*kv)+vgq)*(N*kpv)]);
eqns = subs(eqns, [vdRef w], [eRef-(deltaW/Pmax)*(vCfd*iLrd+vCfq*iLrq), (wRef-(deltaV/Qmax)*(vCfq*iLrd-vCfd*iLrq))]);


% Definition of input and output vectors
x = [iLcd vCfd vCdd iLrd igd m2d vgd iLcq vCfq vCdq iLrq igq m2q vgq];
dx = [diLcd dvCfd dvCdd diLrd digd dm2d dvgd diLcq dvCfq dvCdq diLrq digq dm2q dvgq];

%inputs
u = [eRef, wRef, Zload];

% Solution of the system of equations as a function of the vector dx
S = solve(eqns,dx);
sol = [S.diLcd S.dvCfd S.dvCdd S.diLrd S.digd S.dm2d S.dvgd S.diLcq S.dvCfq S.dvCdq S.diLrq S.digq S.dm2q S.dvgq];

% Linearization of equations
linSol = jacobian(sol,[x,u]);

Alin = linSol(:,1:length(x))
Blin = linSol(:,length(x)+1:end)

% Output equations
eqns_output = [y1 == iLrd,
               y2 == iLrq,
               y3 == vCfd,
```

```
                y4 == vCfq];
% Vector definition
y = [y1, y2, y3, y4];

S_out = solve(eqns_output,y);
sol_out = [S_out.y1, S_out.y2,S_out.y3,S_out.y4];

linSolOut = jacobian(sol_out,[x,u]);

Clin = linSolOut(:,1:length(x))
Dlin = linSolOut(:,length(x)+1:end)

parameters = [Lc, Cf, Cd, Rd, Lr, kpi, Tii, ki, Ts, vqRef,vb, RLc, RLr, kpv, Tiv, kv, Zload, deltaW, Pmax, deltaV, Qmax, eRef, wRef, N]
parameters_value = [294e-6, 27.6e-6, 27.6e-6, 2.26, 294e-6, 0.0031, 1/1e3, 0.470, 1e-5,...
                    0, 120, 0, 0, 2, 1/10, 2, 5, 2*3.14159*2.5, 1500, 6, 500, 62.35, 2*3.14159*50, 2];


% Steady State solution
eqnsSS = subs(eqns,[parameters dx],[parameters_value zeros(1,length(dx))]);
S_SS = solve(eqnsSS,x)
solSS = double([S_SS.iLcd(1) S_SS.vCfd(1) S_SS.vCdd(1) S_SS.iLrd(1) S_SS.igd(1) S_SS.m2d(1) S_SS.vgd(1) S_SS.iLcq(1) S_SS.vCfq(1) S_SS.vCdq(1)
S_SS.iLrq(1) S_SS.igq(1) S_SS.m2q(1) S_SS.vgq(1)]);

% Inputs Vector
uSS = [eRef, wRef, Zload];
uSS = double(subs(uSS,parameters, parameters_value));

% Output solution in steady state
solSS_output = double(subs(Clin,[parameters dx],[parameters_value zeros(1,length(dx))]))*solSS'+...
               double(subs(Dlin,[parameters dx],[parameters_value zeros(1,length(dx))]))*uSS';

%Linearized Matrix
AlinNum = double(subs(Alin, [parameters x], [parameters_value solSS]));
BlinNum = double(subs(Blin, [parameters x], [parameters_value solSS]));
ClinNum = double(subs(Clin, [parameters x], [parameters_value solSS]));
```

```
DlinNum = double(subs(Dlin, [parameters x], [parameters_value solSS]));

% Representation of the small signal model in state space
ssLinSys = ss(AlinNum,BlinNum,ClinNum,DlinNum)

% Stability analysis - Poles
poles = pole(ssLinSys)
```

3. **Generic State Matrices: Inverter with droop control feeding load (Referring to Figure 12)**

Matrix A will be presented in 2 columns at a time, for space reasons. Representation A (:, 1: 2) means: 1st and 2nd column of matrix A, Representation A (:, 3: 4) means: 3rd and 4th column of matrix A, and so on.

$$A(:,1:2) = \begin{bmatrix} \frac{-R_d}{L_c} & \frac{-(Q_max - L_c \Delta E i_{Lcq} i_{Lgq})}{L_c Q_{max}} \\ \frac{1}{C_f} & \frac{(-Q_{max} - C_f R_d \Delta E i_{Lgd} V_{cfq})}{C_f Q_{max} R_d} \\ 0 & \frac{Q_{max} + C_d R_d \Delta E i_{Lgd} V_{cdq}}{C_d Q_{max} R_d} \\ 0 & \frac{L_g \Delta E i_{Lgd}^2 + Q_{max}}{L_g Q_{max}} \\ \frac{K_i}{T_{ii}} & \frac{-(K_i (P_{max} K_{pv} K_v + \Delta\omega i_{Lgd} K_{pv} K_v))}{P_{max} T_{ii}} \\ \frac{-K_i K_{pi}}{T_s} & \frac{-(L_c P_{max} \Delta E i_{Lcq} i_{Lgq} - P_{max} Q_{max} + P_{max} Q_{max} K_i K_{pi} K_{pv} K_v V_{dc} + Q_{max} \Delta\omega i_{Lgd} K_i K_{pi} K_{pv} V_{dc})}{P_{max} Q_{max} T_s V_{dc}} \\ 0 & \frac{-(K_v (P_{max} + \Delta\omega i_{Lgd}))}{P_{max} T_{iv}} \\ \frac{-(L_c Q_{max} \omega_{ref} - L_c \Delta E i_{Lgd} V_{cfq} + L_c \Delta E i_{Lgq} V_{cfd})}{L_c Q_{max}} & \frac{-(\Delta E i_{Lcq} i_{Lgq})}{Q_{max}} \\ 0 & \frac{-(C_f Q_{max} R_d \omega_{ref} - C_f R_d \Delta V i_{Lgd} V_{cfq} + 2 C_f R_d \Delta E i_{Lgq} V_{cfd})}{C_f Q_{max} R_d} \\ 0 & \frac{-(\Delta E i_{Lgq} Vcdd)}{Q_{max}} \\ 0 & \frac{-(\Delta E i_{Lgd} i_{Lgq})}{Q_{max}} \\ 0 & 0 \\ \frac{L_c Q_{max} \omega_{ref} - L_c \Delta E i_{Lgd} V_{cfq} + L_c \Delta_E i_{Lgq} V_{cfd}}{Q_{max} T_s V_{dc}} & \frac{L_c \Delta E i_{Lcd} i_{Lgq}}{Q_{max} T_s V_{dc}} \\ 0 & 0 \end{bmatrix}$$

$$A(:,3:4)=\begin{bmatrix} 0 & \frac{-(\Delta Ei_{Lcq}V_{cfq})}{Q_{max}} \\ \frac{1}{C_fR_d} & \frac{-(C_fR_d\Delta EV_{cfq}^2+Q_{max}R_d)}{C_fQ_{max}R_d} \\ \frac{-1}{C_dR_d} & \frac{-(\Delta EV_{cdq}V_{cfq})}{Q_{max}} \\ 0 & \frac{-(Q_{max}Z_{load}+L_g\Delta Ei_{Lgq}V_{cfq})}{Q_{max}} \\ 0 & \frac{-(\Delta\omega K_iK_{pv}K_vV_{cfd})}{P_{max}T_{ii}} \\ 0 & \frac{L_cP_{max}\Delta Ei_{Lcq}V_{cfq}-Q_{max}\Delta\omega K_iK_{pi}K_{pv}K_vV_{cfd}V_{dc}}{P_{max}Q_{max}T_sV_{dc}} \\ 0 & \frac{-(\Delta\omega K_vV_{cfd})}{P_{max}T_{iv}} \\ 0 & \frac{\Delta Ei_{Lcd}Vcfq}{Q_{max}} \\ 0 & \frac{\Delta EV_{cfd}V_{cfq}}{Q_{max}} \\ \frac{-(C_dQ_{max}R_d\omega_{ref}-C_dR_d\Delta Ei_{Lgd}V_{cfq}+C_dR_d\Delta Ei_{Lgd}V_{cfd})}{C_dQ_{max}R_d} & \frac{\Delta EV_{cdd}V_{cfq}}{Q_{max}} \\ 0 & \frac{-(L_gQ_{max}\omega_{ref}-2L_g\Delta Ei_{Lgd}V_{Cfq}+L_g\Delta Ei_{Lgq}V_{cfd})}{L_gQ_{max}} \\ 0 & 0 \\ 0 & \frac{L_c\Delta Ei_{Lcd}V_{cfq}}{Q_{max}T_sV_{dc}} \\ 0 & 0 \end{bmatrix}$$

$$A(:,5:6) = \begin{bmatrix} 0 & \frac{V_{dc}}{L_c} \\ 0 & 0 \\ 0 & 0 \\ 0 & 0 \\ 0 & 0 \\ \frac{K_{pi}}{T_s} & \frac{-1}{T_s} \\ 0 & 0 \\ 0 & 0 \\ 0 & 0 \\ 0 & 0 \\ 0 & 0 \\ 0 & 0 \\ 0 & 0 \\ 0 & 0 \end{bmatrix}$$

$$A(:,7:8) = \begin{bmatrix} 0 & \frac{L_c Q_{max}\omega_{ref} - L_c \Delta E i_{Lgd} V_{cfq} + L_c \Delta E i_{Lgq} V_{cfd}}{L_c Q_{max}} \\ 0 & 0 \\ 0 & 0 \\ 0 & 0 \\ \frac{K_i K_{pv}}{T_{ii}} & 0 \\ \frac{K_i K_{pi} K_{pv}}{T_s} & \frac{-(L_c P_{max} Q_{max}\omega_{ref} - L_c P_{max} \Delta E i_{Lgd} V_{cfq} + L_c P_{max} \Delta E i_{Lgq} V_{cfd})}{P_{max} Q_{max} T_s V_{dc}} \\ 0 & 0 \\ 0 & 0 \\ 0 & \frac{1}{C_f} \\ 0 & 0 \\ 0 & 0 \\ 0 & \frac{-K_i}{T_{ii}} \\ 0 & \frac{-(K_i K_{pi})}{T_s} \\ 0 & 0 \end{bmatrix}$$

$$A(:,9:10)=\begin{bmatrix}\frac{-(\Delta Ei_{Lcq}i_{Lgd})}{Q_{max}} & 0\\ \frac{C_fQ_{max}R_d\Delta Ei_{Lgd}V_{cfq}-2C_fR_d\Delta Ei_{Lgd}V_{cfq}+C_fR_d\Delta Ei_{Lgq}V_{cfd}}{C_fQ_{max}R_d} & 0\\ \frac{-\Delta Ei_{Lgd}V_{cdq}}{Q_{max}} & \frac{C_dQ_{max}R_d\omega_{ref}-C_dR_d\Delta Ei_{Lgd}V_{cfq}+C_dR_d\Delta Ei_{Lgq}V_{cfd}}{C_dQ_{max}R_d}\\ \frac{-\Delta Ei_{Lgd}i_{Lgq}}{Q_{max}} & 0\\ \frac{-\Delta\omega i_{Lgq}K_iK_{pv}K_v}{P_{max}T_{ii}} & 0\\ \frac{L_cP_{max}\Delta Ei_{Lcq}i_{Lgd}-Q_{max}\Delta\omega i_{Lgq}K_iK_{pi}K_{pv}K_vV_{dc}}{P_{max}Q_{max}T_sV_{dc}} & 0\\ \frac{-(\Delta\omega i_{Lgq}K_v)}{P_{max}T_{iv}} & 0\\ \frac{-(Q_{max}L_c\Delta Ei_{Lcd}i_{Lgd})}{L_cQ_{max}} & 0\\ \frac{-(Q_{max}-C_fR_d\Delta Ei_{Lgd}V_{cfd})}{C_fQ_{max}R_d} & \frac{1}{C_fR_d}\\ \frac{(Q_{max}+C_dR_d\Delta Ei_{Lgd}V_{cdd})}{C_dQ_{max}R_d} & \frac{-1}{C_dR_d}\\ \frac{L_g\Delta Ei_{Lgrd}^2+Q_{max}}{L_gQ_{max}} & 0\\ \frac{-K_iK_{pv}K_v}{T_{ii}} & 0\\ \frac{-(L_c\Delta Ei_{Lcd}i_{Lgd}-Q_{max}+Q_{max}K_iK_{pi}K_{pv}K_vV_{dc})}{Q_{max}T_sV_{dc}} & 0\\ \frac{-K_v}{T_{iv}} & 0\end{bmatrix}$$

$$A(:,11:12)=\begin{bmatrix}\frac{\Delta Ei_{Lcq}V_{cfd}}{Q_{max}} & 0\\ \frac{\Delta EV_{cfd}V_{cfq}}{Q_{max}} & 0\\ \frac{\Delta EV_{cdq}V_{cfd}}{Q_{max}} & 0\\ \frac{L_gQ_{max}\omega_{ref}-L_g\Delta Ei_{Lgd}V_{cfq}+2L_g\Delta Ei_{Lgq}V_{cfd}}{L_gQ_{max}} & 0\\ \frac{-\Delta\omega K_iK_{pv}K_vV_{cfq}}{P_{max}T_{ii}} & 0\\ \frac{-(L_cP_{max}\Delta Ei_{Lcq}V_{cfd}+Q_{max}\Delta\omega K_iK_{pi}K_{pv}K_vV_{cfq}V_{dc})}{P_{max}Q_{max}T_sV_{dc}} & 0\\ \frac{\Delta\omega K_vV_{cfq}}{P_{max}T_{iv}} & 0\\ \frac{\Delta Ei_{Lcd}V_{cfd}}{Q_{max}} & 0\\ \frac{C_fR_d\Delta EV_{cfd}^2+Q_{max}R_d}{C_fQ_{max}R_d} & 0\\ \frac{\Delta EV_{cdd}V_{cfd}}{Q_{max}} & 0\\ \frac{-(Q_{max}Z_{load}L_g\Delta Ei_{Lgd}V_{cfd})}{L_gQ_{max}} & 0\\ 0 & 0\\ \frac{L_c\Delta EI_{Lcd}V_{cfd}}{Q_{max}T_sV_{dc}} & \frac{K_{pi}}{T_s}\\ 0 & 0\end{bmatrix}\quad A(:,13:14)=\begin{bmatrix}0 & 0\\ 0 & 0\\ 0 & 0\\ 0 & 0\\ 0 & 0\\ 0 & 0\\ 0 & 0\\ \frac{V_{dc}}{L_c} & 0\\ 0 & 0\\ 0 & 0\\ 0 & 0\\ 0 & \frac{K_iK_{pv}}{T_{ii}}\\ \frac{-1}{T_s} & \frac{K_iK_{pi}K_{pv}}{T_s}\\ 0 & 0\end{bmatrix}$$

$$B = \begin{bmatrix} 0 & i_{Lcq} & 0 \\ 0 & V_{cfq} & 0 \\ 0 & V_{cdq} & 0 \\ 0 & i_{Lgq} & \frac{-i_{Lgd}}{L_g} \\ \frac{K_i K_{pv} K_v}{T_{ii}} & 0 & 0 \\ \frac{K_i K_{pi} K_{pv} K_v}{T_s} & \frac{-L_c i_{Lcq}}{T_s V_{dc}} & 0 \\ \frac{K_v}{T_{iv}} & 0 & 0 \\ 0 & -i_{Lcd} & 0 \\ 0 & -V_{cfd} & 0 \\ 0 & -V_{cdd} & 0 \\ 0 & -i_{Lgd} & 0 \\ 0 & 0 & 0 \\ 0 & \frac{L_c i_{Lcd}}{T_s V_{dc}} & 0 \\ 0 & 0 & 0 \end{bmatrix}$$

$$C = \begin{bmatrix} 0 & 0 & 0 & 1 & 0 & 0 & 0 & 0 & 0 & 0 & 0 & 0 & 0 & 0 \\ 0 & 0 & 0 & 0 & 0 & 0 & 0 & 0 & 0 & 0 & 1 & 0 & 0 & 0 \\ 0 & 1 & 0 & 0 & 0 & 0 & 0 & 0 & 0 & 0 & 0 & 0 & 0 & 0 \\ 0 & 0 & 0 & 0 & 0 & 0 & 0 & 0 & 1 & 0 & 0 & 0 & 0 & 0 \end{bmatrix}$$

$$D = \begin{bmatrix} 0 & 0 & 0 \\ 0 & 0 & 0 \\ 0 & 0 & 0 \\ 0 & 0 & 0 \end{bmatrix}$$

$State - Space\ Variables$:

$$x = [i_{Lcd} \quad V_{cfd} \quad V_{cdd} \quad i_{Lgd} \quad i_{gd} \quad m_{2d} \quad V_{gd} \quad i_{Lcq} \quad V_{cfq} \quad V_{cdq} \quad i_{Lgq} \quad i_{gq} \quad m_{2q} \quad V_{gq}]$$

$Inputs\ Variables$:

$$u = [E_{ref} \quad \omega_{ref} \quad Z_{load}]$$

$Output\ Variables$:

$$y = [i_{Lgd} \quad i_{Lgq} \quad V_{cfd} \quad V_{cfq}]$$

4. Generic State Matrices: Parallel Inverter System with droop controls (Referring to Figure 27)

Matrix A2 will be presented in 2 columns at a time, for space reasons. Representation A2 (:, 1: 2) means: 1st and 2nd column of matrix A2, Representation A2 (:, 3: 4) means: 3rd and 4th column of matrix A2, and so on.

$$A2(:,1:2)=\begin{bmatrix} \frac{-R_{Lc}}{L_cN} & \frac{-(Q_max-L_c\Delta Ei_{Lcq}i_{Lgq})}{L_cQ_{max}} \\ \frac{1}{C_f} & \frac{(-Q_{max}-C_fR_d\Delta Ei_{Lgd}V_{cfq})}{C_fQ_{max}R_d} \\ 0 & \frac{Q_{max}+C_dR_d\Delta Ei_{Lgd}V_{cdq}}{C_dQ_{max}R_d} \\ 0 & \frac{L_g\Delta Ei_{Lgd}^2+Q_{max}}{L_gQ_{max}} \\ \frac{K_i}{NT_{ii}} & \frac{-(K_i(P_{max}K_{pv}K_v+\Delta\omega i_{Lgd}K_{pv}K_v))}{P_{max}T_{ii}} \\ \frac{-K_iK_{pi}}{N^2T_s} & \frac{-(L_cP_{max}\Delta Ei_{Lcq}i_{Lgq}-P_{max}Q_{max}+P_{max}Q_{max}K_iK_{pi}K_{pv}K_vV_{dc}+Q_{max}\Delta\omega i_{Lgd}K_iK_{pi}K_{pv}V_{dc}}{)}P_{max}Q_{max}T_sV_{dc} \\ 0 & \frac{-(K_v(P_{max}+\Delta\omega i_{Lgd}))}{P_{max}T_{iv}} \\ \frac{-(L_cQ_{max}\omega_{ref}-L_c\Delta Ei_{Lgd}V_{cfq}+L_c\Delta Ei_{Lgq}V_{cfd})}{L_cNQ_{max}} & \frac{-(\Delta Ei_{Lcq}i_{Lgq})}{Q_{max}} \\ 0 & \frac{-(C_fQ_{max}R_d\omega_{ref}-C_fR_d\Delta Vi_{Lgd}V_{cfq}+2C_fR_d\Delta Ei_{Lgq}V_{cfd})}{C_fQ_{max}R_d} \\ 0 & \frac{-(\Delta Ei_{Lgq}Vcdd)}{Q_{max}} \\ 0 & \frac{-(\Delta Ei_{Lgd}i_{Lgq})}{Q_{max}} \\ 0 & 0 \\ \frac{L_cNQ_{max}\omega_{ref}-L_cN\Delta Ei_{Lgd}V_{cfq}+L_cN\Delta_Ei_{Lgq}V_{cfd}}{N^2Q_{max}T_sV_{dc}} & \frac{L_c\Delta Ei_{Lcd}i_{Lgq}}{Q_{max}T_sV_{dc}} \\ 0 & 0 \end{bmatrix}$$

$$A2(:,3:4) = \begin{bmatrix} 0 & \frac{-(\Delta Ei_{Lcq} V_{cfq})}{Q_{max}} \\ \frac{N}{C_f R_d} & \frac{-(C_f R_d \Delta EV_{cfq}^2 + Q_{max} R_d)}{C_f Q_{max} R_d} \\ \frac{-N}{C_d R_d} & \frac{-(\Delta EV_{cdq} V_{cfq})}{Q_{max}} \\ 0 & \frac{-(Q_{max} Z_{load} + L_g \Delta Ei_{Lgq} V_{cfq})}{Q_{max}} \\ 0 & \frac{-(\Delta \omega K_i K_{pv} K_v V_{cfd})}{P_{max} T_{ii}} \\ 0 & \frac{L_c P_{max} \Delta Ei_{Lcq} V_{cfq} - Q_{max} \Delta \omega K_i K_{pi} K_{pv} K_v V_{cfd} V_{dc}}{P_{max} Q_{max} T_s V_{dc}} \\ 0 & \frac{-(\Delta \omega K_v V_{cfd})}{P_{max} T_{iv}} \\ 0 & \frac{\Delta Ei_{Lcd} Vcfq}{Q_{max}} \\ 0 & \frac{\Delta EV_{cfd} V_{cfq}}{Q_{max}} \\ \frac{-N(C_d Q_{max} R_d \omega_{ref} - C_d R_d \Delta Ei_{Lgd} V_{cfq} + C_d R_d \Delta Ei_{Lgd} V_{cfd})}{C_d Q_{max} R_d} & \frac{\Delta EV_{cdd} V_{cfq}}{Q_{max}} \\ 0 & \frac{-(L_g Q_{max} \omega_{ref} - 2L_r \Delta Ei_{Lgd} V_{Cfq} + L_g \Delta Ei_{Lgq} V_{cfd})}{L_g Q_{max}} \\ 0 & 0 \\ 0 & \frac{L_c \Delta Ei_{Lcd} V_{cfq}}{Q_{max} T_s V_{dc}} \\ 0 & 0 \end{bmatrix}$$

$$A2(:,5:6) = \begin{bmatrix} 0 & \frac{V_{dc}}{L_c} \\ 0 & 0 \\ 0 & 0 \\ 0 & 0 \\ 0 & 0 \\ \frac{K_{pi}}{NT_s} & \frac{-1}{T_s} \\ 0 & 0 \\ 0 & 0 \\ 0 & 0 \\ 0 & 0 \\ 0 & 0 \\ 0 & 0 \\ 0 & 0 \\ 0 & 0 \end{bmatrix}$$

$$A2(:,7:8) = \begin{bmatrix} 0 & \dfrac{L_c Q_{max}\omega_{ref} - L_c \Delta E i_{Lgd} V_{cfq} + L_c \Delta E i_{Lgq} V_{cfd}}{L_c N Q_{max}} \\ 0 & 0 \\ 0 & 0 \\ 0 & 0 \\ \dfrac{K_i K_{pv}}{T_{ii}} & 0 \\ \dfrac{K_i K_{pi} K_{pv}}{N T_s} & \dfrac{-(N L_c P_{max} Q_{max}\omega_{ref} - N L_c P_{max} \Delta E i_{Lgd} V_{cfq} + N L_c P_{max} \Delta E i_{Lgq} V_{cfd})}{N^2 P_{max} Q_{max} T_s V_{dc}} \\ 0 & 0 \\ 0 & \dfrac{-R_{LC}}{N L_c} \\ 0 & \dfrac{1}{C_f} \\ 0 & 0 \\ 0 & 0 \\ 0 & \dfrac{-K_i}{N T_{ii}} \\ 0 & \dfrac{-(K_i K_{pi})}{N^2 T_s} \\ 0 & 0 \end{bmatrix}$$

$$A2(:,9:10)=\begin{bmatrix}
\frac{-(\Delta E i_{Lcq} i_{Lgd})}{N Q_{max}} & 0 \\
\frac{N C_f Q_{max} R_d \omega_{ref} - N C_f Q_{max} R_d \Delta E i_{Lgd} V_{cfq} + N C_f R_d \Delta E i_{Lgq} V_{cfd}}{N C_f Q_{max} R_d} & 0 \\
\frac{-N \Delta E i_{Lgd} V_{cdq}}{Q_{max}} & \frac{N(C_d Q_{max} R_d \omega_{ref} - C_d R_d \Delta E i_{Lgd} V_{cfq} + C_d R_d \Delta E i_{Lgq} V_{cfd})}{C_d Q_{max} R_d} \\
\frac{-\Delta E i_{Lgd} i_{Lgq}}{N Q_{max}} & 0 \\
\frac{-N \Delta\omega i_{Lgq} K_i K_{pv} K_v}{P_{max} T_{ii}} & 0 \\
\frac{N L_c P_{max} \Delta E i_{Lcq} i_{Lgd} - N^2 Q_{max} \Delta\omega i_{Lgq} K_i K_{pi} K_{pv} K_v V_{dc}}{N^2 P_{max} Q_{max} T_s V_{dc}} & 0 \\
\frac{-(N \Delta\omega i_{Lgq} K_v)}{P_{max} T_{iv}} & 0 \\
\frac{-(N Q_{max} L_c \Delta E i_{Lcd} i_{Lgd})}{N L_c Q_{max}} & 0 \\
\frac{-N(Q_{max} - C_f R_d \Delta E i_{Lgd} V_{cfd})}{C_f Q_{max} R_d} & \frac{N}{C_f R_d} \\
\frac{(Q_{max} + C_d R_d \Delta E i_{Lgd} V_{cdd})}{C_d Q_{max} R_d} & \frac{-N}{C_d R_d} \\
\frac{L_g \Delta E i_{Lgrd}^2 + N Q_{max}}{L_g N Q_{max}} & 0 \\
\frac{-N K_i K_{pv} K_v}{T_{ii}} & 0 \\
\frac{-(L_c N \Delta E i_{Lcd} i_{Lgd} - N^2 Q_{max} + N^2 Q_{max} K_i K_{pi} K_{pv} K_v V_{dc})}{N^2 Q_{max} T_s V_{dc}} & 0 \\
\frac{-N K_v}{T_{iv}} & 0
\end{bmatrix}$$

$$A2(:,11:12) = \begin{bmatrix} \frac{\Delta E i_{Lcq} V_{cfd}}{N Q_{max}} & 0 \\ \frac{N \Delta E V_{cfd} V_{cfq}}{Q_{max}} & 0 \\ \frac{N \Delta E V_{cdq} V_{cfd}}{Q_{max}} & 0 \\ \frac{L_g Q_{max} \omega_{ref} - L_g \Delta E i_{Lgd} V_{cfq} + 2 L_g \Delta E i_{Lgq} V_{cfd}}{N L_g Q_{max}} & 0 \\ \frac{-N \Delta \omega K_i K_{pv} K_v V_{cfq}}{P_{max} T_{ii}} & 0 \\ \frac{-(L_c N P_{max} \Delta E i_{Lcq} V_{cfd} + N^2 Q_{max} \Delta \omega K_i K_{pi} K_{pv} K_v V_{cfq} V_{dc})}{N^2 P_{max} Q_{max} T_s V_{dc}} & 0 \\ \frac{N \Delta \omega K_v V_{cfq}}{P_{max} T_{iv}} & 0 \\ \frac{\Delta E i_{Lcd} V_{cfd}}{N Q_{max}} & 0 \\ \frac{N C_f R_d \Delta E V_{cfd}^2 + Q_{max} R_d}{C_f Q_{max} R_d} & 0 \\ \frac{N \Delta E V_{cdd} V_{cfd}}{Q_{max}} & 0 \\ \frac{-(N Q_{max} Z_{load} L_g \Delta E i_{Lgd} V_{cfd})}{L_g N Q_{max}} & 0 \\ 0 & 0 \\ \frac{L_c \Delta E I_{Lcd} V_{cfd}}{N Q_{max} T_s V_{dc}} & \frac{K_{pi}}{N T_s} \\ 0 & 0 \end{bmatrix}$$

$$A2(:,13:14) = \begin{bmatrix} 0 & 0 \\ 0 & 0 \\ 0 & 0 \\ 0 & 0 \\ 0 & 0 \\ 0 & 0 \\ 0 & 0 \\ \frac{V_{dc}}{L_c} & 0 \\ 0 & 0 \\ 0 & 0 \\ 0 & 0 \\ 0 & \frac{K_i K_{pv}}{T_{ii}} \\ \frac{-1}{T_s} & \frac{K_i K_{pi} K_{pv}}{N T_s} \\ 0 & 0 \end{bmatrix}$$

$$B2 = \begin{bmatrix} 0 & \frac{i_{Lcq}}{N} & 0 \\ 0 & NV_{cfq} & 0 \\ 0 & NV_{cdq} & 0 \\ 0 & \frac{i_{Lgq}}{N} & \frac{-i_{Lgd}}{L_g} \\ \frac{NK_iK_{pv}K_v}{T_{ii}} & 0 & 0 \\ \frac{K_iK_{pi}K_{pv}K_v}{T_s} & \frac{-L_c i_{Lcq}}{NT_sV_{dc}} & 0 \\ \frac{NK_v}{T_{iv}} & 0 & 0 \\ 0 & \frac{-i_{Lcd}}{N} & 0 \\ 0 & -NV_{cfd} & 0 \\ 0 & -NV_{cdd} & 0 \\ 0 & \frac{-i_{Lgd}}{N} & 0 \\ 0 & 0 & 0 \\ 0 & \frac{L_c i_{Lcd}}{NT_sV_{dc}} & 0 \\ 0 & 0 & 0 \end{bmatrix}$$

$$x2 = [i_{Lcd} \quad V_{cfd} \quad V_{cdd} \quad i_{Lgd} \quad i_{gd} \quad m_{2d} \quad V_{gd} \quad i_{Lcq} \quad V_{cfq} \quad V_{cdq} \quad i_{Lgq} \quad i_{gq} \quad m_{2q} \quad V_{gq}]$$

$$u2 = [E_{ref} \quad \omega_{ref} \quad Z_{load}]$$

$$y2 = [i_{Lgd} \quad i_{Lgq} \quad V_{cfd} \quad V_{cfq}]$$